NTIA Report 99-369

Advanced Antenna Test Bed Characterization for Wideband Wireless Communications

Perry F. Wilson
Peter B. Papazian
Michael G. Cotton
Yeh Lo

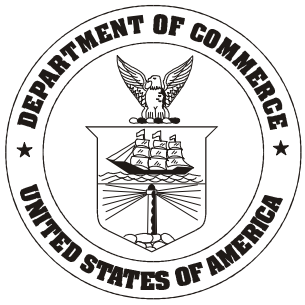

U.S. DEPARTMENT OF COMMERCE
William M. Daley, Secretary

Larry Irving, Assistant Secretary
for Communications and Information

August 1999

This Page Intentionally Left Blank

This Page Intentionally Left Blank

CONTENTS

Page

This Page Intentionally Left Blank

This Page Intentionally Left Blank

LIST OF FIGURES

Page

LIST OF FIGURES (cont'd)

LIST OF TABLES

Page

This Page Intentionally Left Blank

This Page Intentionally Left Blank

ADVANCED ANTENNA TEST BED CHARACTERIZATION FOR WIDEBAND WIRELESS COMMUNICATION SYSTEMS

Perry Wilson, Peter Papazian, Michael Cotton, and Yeh Lo*

An advanced antenna test bed for evaluating adaptive antennas and next-generation mobile communication systems is described. The key elements of the data acquisition system are 8 simultaneous channels, broadband impulse channel sounding, high speed analog to digital data conversion and storage, and flexible post processing. Mobile channel sounding measurements were made in two sectors at 1920 MHz using 4 receiving antennas. Received signal strength and transmission loss are examined. Path loss exponents for the two sectors are found to be 4.89 and 4.08. These are typical for urban to suburban environments. RMS delay spreads for the two sectors are found to be less than 1.38 μs and 0.65 μs at the 90% probability level and 3.14 μs and 1.35 μs at the 99% probability level respectively. Fast fading reduction using antenna diversity (up to 4 antennas) and increased channel bandwidth (19.6 kHz, 1.25 MHz, 5.0 MHz, and 10.0 MHz) is examined. Three signal combining methods are considered: selection diversity, equal gain combining, and maximal ratio combining. Measured results indicate that increasing the number of diversity antennas or the channel bandwidth significantly reduces fading. Maximal ratio combining yields the largest diversity gain exceeding 11.0 dB and 17.0 dB at the 90% and 99% fast fade depth probability levels respectively when all four channels are used.

Key Words: adaptive antennas; advanced antenna test bed; equal gain combining; fast signal fading; impulse channel sounding; maximal ratio combining; power delay profiles; RMS delay spread; selection diversity; transmission loss; wideband measurements

1. INTRODUCTION

Adaptive, active, or “smart” antennas can continuously change their radiation pattern as needed for optimum performance. Wideband wireless communication systems can use adaptive antennas to track a mobile user. Adaptive antennas thus have the potential to increase service capacity and the performance/cost ratio for a number of land-mobile radio systems, including cellular telephone and personal communication service (PCS). A number of researchers are working on adaptive antenna technology, and several adaptive antenna systems are being developed and marketed. However, common, realistic methods for testing the comparative performance of systems and signal processing algorithms are

* The authors are with the Institute for Telecommunication Sciences, National Telecommunications and Information Administration, U.S. Department of Commerce, Boulder, CO 80303

not available. A standardized measurement process and test environment is necessary before the cost benefits of these complex systems can be assessed.

This report describes an advanced antenna test bed (ATB) developed by the Institute for Telecommunication Sciences (ITS) which can be used for the comparative testing of adaptive systems and data processing algorithms. Central to the metrology is a realistic, well defined test cell and a multi-channel, high-bandwidth measurement system. The ATB uses the Green Mountain Mesa (GMM) cell which is part of the Boulder Industry Test Bed (BITB). The BITB provided a common environment for the field testing of PCS air-interface standards by the Joint Technical Committee (JTC) on Wireless Access. A summary of these tests has been prepared by Wepman [1]. Measurement results for all the current PCS standards are available and can be used for comparison with advanced antenna tests. The wideband measurements reported here also serve as a base line for measuring the performance of advanced antennas and systems.

The report is organized as follows. Section 2 gives a brief description of the ATB digital channel probe. The channel probe uses a spread spectrum measurement technique to approximate the impulse response of a radio channel over a large bandwidth. Impulse response data are used to characterize the propagation environment of the GMM cell, as detailed in Section 3. Signal strength (peak impulse power), as a function of position in the cell, and basic transmission loss, versus transmitter-to-receiver separation, are examined. Section 4 uses the impulse data to generate delay statistics for the cell. Minimum delay, mean delay, and delay spread are considered. In addition, diversity gain in the form of best channel (least delay spread) versus mean channel performance is investigated. Section 5 uses the impulse power spectral density (PSD) data to evaluate fading reduction and diversity gain for a narrowband signal and three wideband signals. Various antenna combinations (1-4 antennas) are also examined for the four signal bandwidths. The bandwidths were chosen to match the existing CDMA and wideband CDMA standards. Section 6 summarizes the results.

2. MEASUREMENT SYSTEM DESCRIPTION

The ATB uses an upgraded version of the Institute for Telecommunication Sciences (ITS) digital channel probe (DCP). This probe has been used to make impulse response measurements in the 900-MHz cellular and 1900-MHz PCS bands [2-3]. The DCP transmits a maximal-length pseudo-noise (PN) code. The PN code is used to biphase shift key (BPSK) modulate the RF carrier. The transmitter is both frequency and bit-rate agile and can produce multiple PN codes and frequencies simultaneously. This is useful for polarization and spatial diversity studies.

The transmitted signal, modified by the radio channel, is received, down-converted to an intermediate frequency (IF), and then digitized. If desired, the in-phase and quadrature-phase components can then be determined via software. A complex impulse response can be generated by cross-correlating a copy of the transmitted PN code with the received signal after down-conversion to baseband using software. Because the DCP digitizes at

IF, it can measure an impulse response much faster than an analog sliding correlator. In particular, the time window for this digital system is the length of one PN code whereas the time window for an analog sliding correlator is some larger multiple (>1) of the PN code length [4]. This allows better characterization of a rapidly changing radio channel. It also avoids problems with nonlinear components when making wideband measurements and allows accurate wideband amplitude and phase calibration of the system. This is essential for digital beam-forming applications.

The probe is currently configured to transmit a 511 bit PN word at 10 Mb/s using a 1.92 GHz carrier. The theoretical impulse signal power to correlation noise power level is 54 dB for the 511 bit PN sequence. The processing gain of the system is 27 dB when the signal power equals the noise power. Multipath signals separated by 100 ns can be resolved to a maximum delay of 51 μs using this setup. A nominally flat 12 MHz bandwidth power spectral density (PSD) spectrum results after normalizing to a calibration curve. The 12 MHz bandwidth is approximately the –10 dB roll-off of the calibration PSD. The probe can also be configured for higher bit rates (higher bandwidth and time resolution), longer codes (longer maximum delays), different code types and other RF carriers. Additional features of the system include time of flight and Doppler measurements. System timing is maintained using rubidium oscillators at the transmitter and receiver. These clocks synchronize the PN code generators, phase lock all local oscillators and provide sampling clocks for the digitizers. Multiple digital signal processors (DSPs) and a host computer system control data acquisition. The DSPs can be configured for real time processing or data streaming.

For these tests, data acquisition was set to the burst mode. In this mode a burst of data is collected in rapid sequence and stamped with GPS coordinates and time. The next data burst is acquired after a programmable delay which was set to 3 seconds. Within a burst, the delay between impulses was set to 3 ms. This high resolution enables Doppler spectrum measurements. The number of impulses per burst was set to 128, resulting in an overall burst duration of approximately 388 ms. For typical vehicle speeds a burst covered from 20-60 wavelengths. This is important when analyzing narrowband fading. By using the vehicular velocity from the GPS data, log normal (slow fading) could be averaged out from the narrowband data leaving only the fast fading components.

Table 1 below summarizes the data acquisition parameters used for the diversity measurements as well as the range of permissible values for the ATB system. Block diagrams for the system can be found in [5].

A mobile transmitting antenna and a fixed receiving antenna array were used. The mobile transmitter used an omni-directional dipole antenna with 6.7 dBi gain and 17.5° vertical beamwidth. This antenna was mounted at a height of 2.4 m on a van equipped with a GPS/dead reckoning system. The maximum transmitter power is 10 W. The receiving array consisted of four PCS flat panel antennas horizontally spaced 2λ, 3λ, and 5λ apart. The antenna array is shown in Figure 1. The 3 dB azimuthal beamwidth of each antenna is 86° and the vertical beamwidth is 8°. The nominal gain for each antenna is 14 dBi.

Table 1. Data Acquisition and RF Parameters used for Diversity Tests

Configurable System Parameters		
Parameter	Diversity Tests	ATB System
Receiver Channels	4	1-8
Carrier Frequency	1.92 GHz	.45 – 6 GHz
Bit Rate	10 Mb/s	.1 – 50 Mb/s
Resolution	100 ns	10 μs – 20 ns
Code Type	Maximal Length	Programmable
Code Length	511 bits	Programmable
Acquisition Mode	Burst	Continuous or Burst
Positioning	GPS/Dead Reckoning	GPS/Dead Reckoning
Transmitters	1	Multiple
Data Processing	Post	Post or Real Time

The range of the system may be estimated using a modification of the free space path loss equation

$$\frac{p_r}{p_t} = g_r g_t \left(\frac{l}{4pd} \right)^2 \quad , \tag{1}$$

where p_r and p_t are the received and transmitted powers, g_r and g_t are the receive and transmit antenna gains, and d is the separation. In a real environment the path loss will be greater than in free space due to obstacles. Path loss (PL) exponents n are typically in the range 2-4 with 3.5 typical for a suburban environment. The free space equation may be modified to include a short free space path length d_0 to account for the raised receive antenna followed by a path length d/d_0 (assuming $d > d_0$) with a path loss exponent n [6]

$$\frac{p_r}{p_t} = g_r g_t \left(\frac{l}{4pd} \right)^2 = g_r g_t \left(\frac{l}{4pd_0} \right)^2 \left(\frac{d_0}{d} \right)^2 \rightarrow g_r g_t \left(\frac{l}{4pd_0} \right)^2 \left(\frac{d_0}{d} \right)^n . \tag{2}$$

Expressed in dBs (upper cases), (2) can be written as follows

$$\begin{aligned} PL &= P_t - P_r + G_t + G_r = PL_{fs}(d_0) + PL_n(d/d_0) \\ PL_{fs}(d) &= 20\log_{10}(4pd/l) \\ PL_n(d) &= 10n\log_{10}(d) \end{aligned} \quad , \tag{3}$$

where the subscript *fs* denotes the free space path loss (isotropic antennas) and the subscript *n* indicates an exponent average received signal power decrease. Consider the following range estimate: P_t = 35 dBm (the transmitter is typically driven below the 40 dBm (10 W) maximum power to avoid non-linearities), P_r = -90 dBm (the end of the linear receiver

calibration range although –98 dBm is possible), G_t = 3.7 dBi (6.7 dBi antenna gain less 3 dB cable loss), G_r = 12 dBi (14 dBi antenna gain less 2 dB cable loss), d_0 = 100 m (approximate clear line of sight), and n = 3.5 (typical for suburban environments). Inserting these and solving for d yields approximately 6 km. This range is consistent with the measurement results presented here. A pure free space environment (n = 2) would yield a range on the order of 135 km.

The variable antenna spacing was chosen so that channel independence as a function of antenna spacing can be examined. A typical rule in mobile communications is to use at least a 10λ spacing to ensure channel independence. In applications where space is limited narrower separations would be desirable. The array here allows separations of 2λ, 3λ, 5λ, 8λ, and 10λ to be considered. Channel independence, as a function of antenna spacing, will be the topic of a separate investigation. Within this report it will be assumed that channels are approximately independent when combining them for diversity statistics. This may be a poor assumption in the 2λ separation case. However, the 10λ separation is always considered as well and provides a reasonable check.

The system is calibrated in a back-to-back mode during field testing. When calibrating, the transmitter maximum non-compressed output power is routed via a fixed attenuator, variable attenuator, directional coupler and a power splitter to each receiver channel. The variable attenuator is used to adjust the input power over the dynamic range of the system and a power meter is used to monitor input power. The transmitter used a 2.5 W linear amplifier. The maximum input power was set at –35 dBm per channel and the dynamic range of the AGC amplifiers is 60 dB. The sensitivity of the system for a 20 MHz bandwidth is –98 dBm and the processing gain for the 511 bit code is 27 dB, as discussed above. By calibrating from –35 to –115 dBm, system performance can be monitored from the maximum input signal to noise. Figure 2 shows a sample calibration impulse (no propagation channel). The impulse well approximates the triangular shape of an ideal autocorrelated PN code and the 52 dB peak closely approaches the 54 dB theoretical limit.

Figure 3 shows an example of a signal after mobile channel propagation. Such received impulses form the basis for the statistics that follow. For this example the power delay profile (PDP) shows significant multipath (a). The received signal strength (RSS) discussed in Section 3 is the PDP peak. The delay statistics in Section 4 are based on the PDP spread. It should be noted that the delay statistics presented in Section 4 are based on the full impulse data and thus the 20 MHz null-to-null bandwidth shown in (b). The PSD (b) can be normalized by a calibration impulse PSD (c) resulting in a normalized PSD (d). The apparent frequency selective fading near the +/- 10 MHz edges of the normalized PSD is due to poor signal-to-noise ratio (S/N) and does not represent usable data. The usable bandwidth for the configuration used in this report is on the order of 12-15 MHz. The fading statistics in Section 5 are based on normalized PSDs (NPSDs).

3. CELL DESCRIPTION

The ATB utilizes the Green Mountain Mesa (GMM) cell of the BITB. During the BITB study [1] the GMM cell receiver was located on a hilltop, 120 m above the Boulder Valley floor, within a large open area in a suburban residential section of Boulder. For the tests reported here, the receiving antenna site was moved to the roof of wing 4 of the Radio Building on the Department of Commerce (DOC) Campus. This put the base of the site 14 m above the floor of Boulder Valley. The base elevation for this site is 1651 m and the antenna array height is 6.7 m above the base. The GMM cell is essentially east of the DOC location. Measurements to the west are not feasible because the foothills of the Rocky Mountains rise rapidly to the west of the DOC campus.

The GMM site is a typical suburban environment with moderate delay spreads and moderate to high path loss. To characterize the test area, the received signal strength (peak impulse power) and basic transmission loss were measured for two GMM cell sectors. A map showing the ITS (receiver) location, the two drive routes (sectors), and the RSS is shown in Figure 4. The drive routes were selected to maximize data quality and the percentage of data with acceptable S/N, as needed for delay spread and normalized power spectral density calculations. A main NW-SE artery (US 36) separates the two drive routes. For the route north of US 36 the antenna array normal was directed 47° north of east (approximately NE) and for the south route the array normal was directed 13° south of east. For simplicity the two routes will be designated NE and SE respectively in the discussion that follows.

The RSS data were used to calculate the basic transmission loss (L_{bt}) for the NE and SE sectors, as shown in Figures 5-6. The transmission loss data shown are based on the local mean RSS for each burst (averaged over the 128 impulses). The data are plotted versus distance on a log scale. Also shown is a linear curve fit (least squares) of the form

$$y = n10\log_{10}(d) + b \qquad (4)$$

which represents the non free space path loss in equation (3) above. Using this fit, the basic transmission loss has a slope *n* of 4.89 for the NE sector and 4.08 for the SE sector. These are typical for low antenna heights in the 1.9 GHz band [6-7].

4. DELAY SPREAD

The delay statistics presented in this report are based on averaged power delay profiles (APDPs)

$$APDP(t_i) = \frac{1}{N}\sum_{k=1}^{N} PDP_k(t_i) \quad , \tag{5}$$

where t_i is the i-th time step (sampling point), and N is the number of PDPs used to form the APDP. APDPs are used to reduce the noise effects. The present ATB burst configuration software sets the number of impulses in a burst to a power of 2, typically 32, 64, or 128 (overall range 1-256). APDPs are calculated from a group of 8 successive PDPs similar to the 10 PDPs used in previous studies [2-3]. The choice of 8 as the group size makes efficient use of all the burst data. APDPs are computed separately for each channel.

4.1 APDP Analysis

Impulses within an APDP group (8 successive PDPs) are first checked for sufficient power. The impulse with the maximum total signal power is found by integration over the full time interval. Impulses with total signal powers more than 10 dB below this group maximum are discarded for the APDP statistics. Groups containing less than 4 usable impulses are discarded as well. Thus, N ranges from 4 to 8 in (5) above. Valid impulses within a group are next aligned with the maximum impulse. Alignment is achieved by calculating the cross correlation and then time shifting each valid impulse accordingly. The aligned impulses are then averaged via (5) to form the APDP.

The interval of discrimination (ID) is here defined as the difference in power levels between the peak of the intended signal (impulse) and the peak noise. It is desired that an APDP have an ID of at least 20 dB to insure that noise is not calculated into the fading statistics. A 23 dB ID criterion will be used. A difficulty is determining the end of the intended signal and the beginning of noise only. It is assumed here that the impulse occurs near the beginning of the 51 μs time interval so that the last 10% of the time interval captured may be considered noise. Most meaningful multipath signals should reach the receiver within 20 μs of the shortest path signal. This corresponds to an increased path length of 6 km. Signals arriving later than 46 μs (final 10%) should be sufficiently attenuated so as not to be of interest. Absolute time synchronization between the transmitter and the receiver allows the impulse trigger of the transmitted signal to be positioned at the beginning of the captured time interval. Thus, the ID is determined here by comparing the APDP peak during the first 90% of the measured time interval to the APDP peak during the last 10% of the measured time interval. If the ID is less than 23 dB the APDP is discarded.

Although a 23 dB ID criterion has been applied to the APDP, only signal levels within 20 dB of the APDP peak are included in the delay statistics. Thus, for each valid APDP the

signal of interest is determined and then time shifted such that the impulse begins at time zero. These corrected APDPs are the basis for all delay spread statistics that follow. Figure 7 shows an example of a raw and a corrected APDP. For this APDP only the first echo beyond the initial signal is retained for the delay statistics.

Data are presented in two groups based on two GMM cell sectors. These are designated NE and SE, as discussed above (see Figure 4). The sectors were measured using 220 and 216 bursts respectively. Each burst consisted of 128 impulses on 4 simultaneous channels. Thus, the two basic data sets consist of 112,640 (SE) and 110,592 (NE) impulses resulting in 14,080 and 13,824 APDPs respectively. Of these APDPs, 8286/14,080 (59%) and 8735/13,824 (63%) are found to be valid under the constraints described above. The valid APDPs' peak powers for the NE and SE drives are shown in Figures 8-9. The NE drive (Figure 8) is basically an out and back route relative to the receiving antenna. The SE drive data (Figure 9) are somewhat discontinuous with a larger segment of the drive at a relatively far distance compared to the NE drive. The NE drive is largely toward lower elevations (creek valley) and the SE drive is more toward higher elevations (with respect to the receiving antenna). Thus, we expect more line of sight paths for the SE drive.

4.2 Statistics

Three delay measures will be considered: maximum delay, mean delay, and RMS delay spread. These will be based on the corrected APDPs. The data from all 4 channels are combined together in a single data set for the purpose of the delay statistics.

The maximum delay is here defined as the time delay between the first and last signals of the corrected APDPs. Since the corrected APDPs have been shifted so that the initial signal occurs at $t = 0$, the maximum delay is equivalent to the length of the corrected APDP (see Figure 7).

The mean delay (d) is the time weighted average, or first moment, of the corrected APDPs normalized by the average signal power,

$$mean\ delay = d = \frac{\frac{1}{N}\sum_{k=1}^{N} t_k P(t_k)}{\frac{1}{N}\sum_{k=1}^{N} P(t_k)} = \frac{\sum_{k=1}^{N} t_k P(t_k)}{\sum_{k=1}^{N} P(t_k)} \quad , \tag{6}$$

where t_k is the time delay (in seconds) relative to the start of the corrected APDP (i.e., $t = 0$), P is the signal power (W), and N is the index of the final corrected APDP signal point considered.

The RMS delay spread (S) measures the standard deviation of the delay spread of each corrected APDP about its mean delay (d). It is the second central moment of the corrected APDP given by

$$RMS\ delay\ spread = S = \left[\frac{\sum_{k=1}^{N} (t_k - d)^2 P(t_k)}{\sum_{k=1}^{N} P(t_k)} \right]^{1/2} \quad . \qquad (7)$$

Figures 10-11 show the cumulative probability distributions for the NE amd SE data maximum delay, mean delay, and RMS delay spread. The NE data show more multipath than the SE data as expected from the terrain profile discussed above. The data here are plotted on the same scale as in [3, Figures 5.4-5.6] for comparison, and fall somewhere between the hilly rural cell and the urban high-rise cell. This is most clear for the NE sector data set. The NE sector, while primarily suburban, does feature some large buildings (reflectors) along with undulating terrain. Thus, the result is consistent with the previous measurements.

4.3 Spatial Diversity

Spatial diversity may be used to improve the delay statistics by choosing the APDP with the least delay effect from the 4 available channels. This assumes that at least two of the APDPs are valid. The best channel can be compared to the individual channels, or to the mean of the 4 channels (valid APDPs only). For this study, the latter choice is used. Only cases where at least two of the APDPs are valid are included in the statistics.

Figures 12-13 show the cumulative probability distributions for the NE and SE data sets where the channel with the best (least) delay spread statistics is compared to the mean of the valid channels (for each group). The diversity gain is greater for the NE data than for the SE data as is expected from the overall delay statistics shown in the previous two figures.

5. FAST FADING

This section examines the effect of bandwidth and spatial diversity on signal fading. The statistics will be based on the normalized power spectral density (NPSD) of the measured impulses. The NPSD is here defined as the magnitude squared of the discrete Fourier transform (DFT) of an impulse signal (or delay profile (DP)) normalized to the magnitude squared of the DFT of a calibration impulse (CAL_DP).

$$NPSD = \frac{\left[DFT(DP)\right]^2}{\left[DFT(CAL\_DP)\right]^2} \quad . \qquad (8)$$
$$PDP(t_i) = DP(t_i)^2$$

The PDPs discussed in the last section are simply the squares of the DPs. An example of an NPSD is shown in Figure 3(d).

5.1 Frequency Selective Fading versus Bandwidth

Four bandwidths will be considered: 19.6 kHz, 1.25 MHz, 5.0 MHz, and 10 MHz. The first of these, 19.6 kHz, represents the minimal bandwidth possible for the measurement system configuration chosen here and will be considered an approximate narrowband continuous wave (CW) signal. The three larger bandwidths are representative of broadband channels used for CDMA. Note that all four bandwidths are based on the same measured NPSDs and differ only in the number of data points about the center frequency used for the analysis.

It is expected that fading should be frequency selective. Thus, signal power r over a broad bandwidth,

$$r(BW) = \int_{f_0 - BW/2}^{f_0 + BW/2} NPSD(f)df \,, \tag{9}$$

should be less influenced by fading than signal power over a narrow bandwidth. In (9), BW is the bandwidth, f_0 is the carrier frequency (typically the data have been demodulated to baseband and f_0 may be replaced by 0), and $NPSD(f)$ is the normalized PSD as a function of frequency. Note that the integral is actually a summation over the sampled bandwidth.

For the four bandwidths considered here we expect the 19.6 kHz signal to exhibit the most fading and the 10 MHz signal to exhibit the least fading. Fading reduction should be largest for the initial bandwidth increase (e.g., 19.6 kHz to 5.0 MHz).

Figure 14 shows $r(BW)$ for a typical burst (NE Burst 1). The four bandwidths are plotted for each of the four channels. As expected, fading is strongest for the 19.6 kHz narrowband case (blue line). The 5 MHz data (red line) already show considerably less variation. Reduced fading with increased bandwidth implies that gains from spatial diversity are exected to be similarly reduced.

An alternate method to view the bandwidth effect on fading is to consider the data density distribution. Figures 15 and 16 show the distribution of signals about their local mean (discussed in the next section) expressed in dB (the local mean is used as the 0 dB reference level). The data from all four channels are grouped into a single data set. Both the NE (Figure 15) and SE (Figure 16) data demonstrate that as the bandwidth is increased the distribution narrows, implying less fading.

5.2 Spatial Diversity – General Comments

Signals from multiple antennas, or "diversity," can be used to reduce the effects of fading. Assuming that the signals from multiple antennas are independent, thus experiencing fade at different times and frequencies, the combined signal should have a lower probability of a given fade level than the individual signals. The more independent channels used, the better the fade reduction. Three common combining schemes are investigated here, namely, selection diversity (SD), equal gain combining (EG), and maximal ratio combining (MR). The combining analysis is performed on the post processed channel signals $r_i(BW)$, where i denotes the channel number. We begin with a brief review of these three techniques.

For any given impulse, the signal voltages v_i ($r_i = |v_i|^2$) from the multiple antennas are combined as follows,

$$\begin{aligned} r &= \left(\max_i |v_i|\right)^2 = \max_i (r_i) && \text{selection diversity} \\ r &= \frac{1}{M}\left(\sum_{i=1}^{M} |v_i|\right)^2 && \text{equal gain} \\ r &= \sum_{i=1}^{M} |v_i|^2 = \sum_{i=1}^{M} r_i && \text{maximal ratio} \end{aligned} \quad . \qquad (10)$$

Thus, selection diversity chooses the strongest signal (only a single signal is used if identical signal levels occur), equal gain combines the cophased signal voltages with equal weights, and maximal ratio weights the cophased signal voltage by itself, equivalent to a sum of the signal powers. Note that maximal ratio combining should weight signal voltages according to their relative signal to noise ratio [8]; however, as the noise may not be known a priori, signal strength alone is used here.

5.3 Fast Fading Statistics and Burst Duration

The fading reduction resulting from the various schemes will be examined as follows. A signal r may be expressed as the product of its local mean m and a fast fading contribution f [8,10],

$$r = mf \quad , \qquad (11)$$

where r can represent both a signal from an individual channel and a combined signal.

The local mean m varies slowly as a function of terrain and possible time dependent medium changes (e.g., rain, foliage), but is essentially stationary over short path lengths and times. The fast fading portion f of the signal includes the rapid variations due to multipath and other non quasi-static contributions (e.g., moving reflectors). If the local mean is known then the fast fading portion is simply

$$f = \frac{r}{m} \quad . \tag{12}$$

The local mean is found by averaging over some path length about the point of interest, or equivalently to a time duration for a moving transmitter [11],

$$m = \frac{1}{P}\int_P r(x)dx \quad , \tag{13}$$

where P describes the path length of interest. The choice of P is nontrivial in that if P is too short then the local mean may not be accurately estimated and if P is too large then slow fade terrain effects may be incorrectly included in the local average. An accepted length used for P is 40 λ [8]; however, a range about this value should give good results. Lengths of 20-50 λ are suggested in [8]. Assuming the mean is constant over such a path (P) implies that

$$m = \frac{1}{P}\int_P r(x)dx = \frac{1}{P}\int_P mf(x)dx = m\frac{1}{P}\int_P f(x)dx \quad . \tag{14}$$

Thus, for the definition here the expected value of the fast fade contribution is unity.

Fast fading statistics will be based on f as expressed in dB. The statistics are generated as follows. Data were collected in the burst mode. The distance covered during a burst (128 impulses, approx. 0.4 s duration) is proportional to the velocity of the mobile transmitter (assumed constant during the burst). Each burst is checked for path length. Bursts covering path lengths between 20 λ and 50 λ are considered valid and included in the statistics. Invalid bursts are discarded. Figures 17 and 18 show the path length per burst for the two data sets (NE, SE). For the NE data 118/220 bursts satisfy the path length requirement while for the SE data 132/216 bursts do so. Note that few paths exceed 40 λ; thus, the 20-50 λ range suggested in [8] is largely adhered to. For each valid path (burst of 128 impulses) the mean of the signal power (9) over the path is calculated via (14). This represents the local mean. The burst signal is then normalized to this local mean to determine the fast fading portion of the signal.

Invalid bursts are typically due to insufficient vehicle speed resulting in a short path. Figure 19 shows the straight line path length in wavelengths versus vehicle speed for burst durations from 0.2 s to 1.0 s in 0.2 s steps. Also shown are the data points per wavelength for a 128 impulse burst for the same range of values. The choice of burst duration must balance the requirement of a minimum path length (minimum duration) and sufficient sampling density (maximum duration). The data here were collected primarily in suburban areas. Thus, typical vehicle speeds were 30-70 kph. Figure 19

(upper) indicates that at least a 0.4 s burst duration is necessary; however, burst durations above 0.6 s would yield excessive path lengths over much of the expected speed range (the desired 20-50 λ path length boundaries are plotted on the graph). Figure 19 (lower) shows that burst durations longer than 0.4 s will yield insufficient sampling density over much of the expected speed range (the desired 3-5 samples per λ boundaries are plotted on the graph). Thus, the 0.377 s burst duration is a reasonable choice for the vehicle speeds typical of a suburban environment.

For usable bursts (valid path length), channels are combined as outlined above (the three weighting schemes) and normalized to the local mean of a single channel [9]. Channel 1, the leftmost antenna in Figure 1, will be used as the reference channel. Statistics will be expressed in terms of the fast fading cumulative distribution functions (CDFs), i.e., the probability that f (in dB) is less than a given level. Gain is then defined as the difference in levels for a given probability. The computed gain for the various combining schemes, channel numbers, and bandwidths will be in reference to channel 1 data.

5.4 Channel Equivalence

Effective fading reduction via spatial diversity assumes that the channels are equivalent (similar means) and uncorrelated. As stated, the four antennas used here are located at distances of 2λ, 5λ, and 10λ with reference to antenna 1. Equivalence can be checked by comparing the CDFs of the four antennas for the four bandwidths. These data are shown in Figure 20. The channels exhibit similar fading with some minor exceptions, namely, NE channel 2 (blue) for 19.6 kHz, NE and SE channel 3 (red) for 1.25 MHz, and SE channel 4 (green) for 10 MHz. Larger bandwidths yield more compressed distributions. The narrowband data for both the NE and SE data sets are very similar. However, the broadband data show noticeably more fading for the SE data set.

5.5 Spatial Diversity – Results of Measured Data

Figure 21 shows selection diversity gain for various channel combinations in the form of CDF plots. In each case, the reference is channel 1 (no diversity, black line). Considered are channel 1 combined individually with channels 2, 3, and 4 (2λ, 5λ, 10λ separation respectively, blue lines), as well as three (123, 124, 134, red lines) and four (1234, green line) channel combinations. The diversity gain is equivalent to the difference between curves for a given probability (horizontal offset). In the narrowband case, diversity gain increases as more channels are combined, as expected. The largest increase is from 1 to 2 channels (black to blue) with lesser gains for further increases. Diversity gain decreases as bandwidth is increased, also as expected. For the NE data, selection diversity results in little gain for the 5 MHz and above bandwidths. The increased fading for the SE data results in better selection diversity gain; however, the trend is the same.

Equal gain combining yielded larger gains than did selection diversity, as shown in Figure 22. Again, the narrowband data show the largest gains. However, wider

bandwidths also exhibit notable gain. This is primarily a result of increased signal strength (multiple channels are summed) relative to the single channel local mean rather than fast fading reduction. Figure 23 shows the CDFs for signals combined via the maximal ratio scheme outlined above. The results are very similar to the equal gain case. For a narrowband, Rayleigh distributed signal, we expect that maximal ratio combining should yield larger gains than equal gain combining and selection diversity, in that order [9], with equal gain and maximal ratio being nearly equivalent. The data here follow this trend.

Figures 24-26 show the two channel, three channel, and four channel CDFs for the three techniques (an alternate representation of the data in Figures 21-23). The figures indicate the ordering in combining technique gains. The data are summarized in Tables 2 and 3 which give the gains for the various channel combinations and combining techniques at the 90% and 99% probabilty levels (the probability that the fade depth exceeds a given signal level). As discussed, the largest gains are for the narrowband case with 90% probability maximal ratio combining gains exceeding 11 dB and the 99% probability maximal ratio combining gains exceeding 17 dB when all four channels are used.

6. CONCLUSION

The ATB system has been used to define propagation conditions in the GMM cell. Two GMM sectors, designated NE and SE, have been studied. Log-log plot slopes for the basic transmission loss versus distance are found to be 4.9 and 4.1 in the NE and SE sectors. NE sector RMS delay spreads are found to be less than 1.38 μs and 3.14 μs at the 90% and 99% probability levels while SE sector RMS delay spreads are found to be less than 0.65 μs and 1.35 μs at the 90% and 99% probability levels. Both the basic transmission loss and RMS delay spread results are consistent with previously published PCS data for a suburban to urban environment.

In addition the GMM cell has been characterized using diversity combining techniques at multiple bandwidths. As expected, it was found that diversity gain is greatest for narrowband signals. Increasing the bandwidth (1.25 MHz, 5.0 MHz and 10 MHz were considered) reduces the diversity gain. These data will aid in the testing of beam forming based advanced antenna systems and processing algorithms.

Table 2. The 90% Fade Level Diversity Gain (dB)

	90%							
	NE				SE			
	19.6 kHz	1.25 MHz	5.0 MHz	10.0 MHz	19.5 kHz	1.25 MHz	5.0 MHz	10.0 MHz
2 Channels								
SD12	5.3	2.2	1.5	1.3	5.0	2.4	1.6	1.3
EG12	6.3	4.3	3.8	3.6	6.0	4.1	3.7	3.4
MR12	6.8	4.4	3.9	3.7	6.5	4.3	3.8	3.5
SD13	4.9	1.7	1.1	0.9	4.8	2.0	1.5	1.2
EG13	5.8	3.7	3.4	3.3	5.7	3.9	3.5	3.4
MR13	6.4	3.9	3.5	3.4	6.2	4.1	3.6	3.5
SD14	5.2	2.1	1.5	1.2	5.3	2.5	1.8	1.5
EG14	6.1	4.1	3.6	3.4	6.2	4.3	3.9	3.7
MR14	6.4	4.2	3.7	3.5	6.8	4.5	4.1	3.8
3 Channels								
SD123	6.7	2.7	1.9	1.6	6.6	3.0	2.2	1.8
EG123	8.7	6.0	5.5	5.4	8.4	6.0	5.4	5.2
MR123	9.4	6.2	5.6	5.5	9.1	6.3	5.6	5.4
SD124	7.2	3.0	2.1	1.7	7.1	3.5	2.6	2.2
EG124	8.9	6.3	5.7	5.4	8.9	6.5	5.9	5.6
MR124	9.7	6.5	5.8	5.5	9.6	6.8	6.1	5.7
SD134	6.7	2.6	1.8	1.4	6.8	3.2	2.3	1.8
EG134	8.4	5.8	5.3	5.1	8.5	6.2	5.6	5.4
MR134	9.2	6.1	5.5	5.3	9.2	6.4	5.8	5.6
4 Channels								
SD1234	7.8	3.2	2.2	1.9	7.8	3.9	2.8	2.3
EG1234	10.4	7.4	6.8	6.6	10.3	7.7	7.0	6.7
MR1234	11.2	7.6	7.0	6.7	11.1	8.0	7.2	6.9

Table 3. The 99% Fade Level Diversity Gain (dB)

	99%							
	NE				SE			
	19.6 kHz	1.25 MHz	5.0 MHz	10.0 MHz	19.5 kHz	1.25 MHz	5.0 MHz	10.0 MHz
2 Channels								
SD12	10.5	2.6	1.8	1.3	9.4	3.7	2.7	2.1
EG12	11.2	4.7	4.1	3.7	10.3	5.5	4.5	3.9
MR12	11.9	4.8	4.2	3.8	10.9	5.8	4.7	4.0
SD13	10.4	2.2	1.5	1.0	9.2	3.6	2.9	2.3
EG13	11.3	4.4	3.9	3.6	10.1	5.3	4.8	4.4
MR13	11.8	4.5	4.0	3.6	10.7	5.5	5.0	4.6
SD14	10.5	2.5	1.7	1.3	10.0	4.1	3.2	2.6
EG14	11.2	4.6	3.9	3.5	10.9	5.9	5.1	4.5
MR14	11.8	4.8	4.0	3.6	11.4	6.1	5.3	4.7
3 Channels								
SD123	13.4	3.4	2.3	1.7	12.3	4.9	3.6	3.0
EG123	15.1	6.8	6.0	5.5	14.2	7.6	6.7	6.2
MR123	16.0	7.0	6.1	5.6	14.9	8.0	6.9	6.4
SD124	13.5	3.7	2.6	2.0	12.9	5.5	4.2	3.4
EG124	15.5	7.2	6.1	5.7	14.6	8.4	7.2	6.4
MR124	16.2	7.3	6.2	5.8	15.3	8.7	7.4	6.6
SD134	13.4	3.3	2.1	1.6	12.9	5.3	4.1	3.3
EG134	15.1	6.8	5.9	5.4	14.4	8.1	7.1	6.4
MR134	15.8	7.0	6.0	5.5	15.3	8.4	7.3	6.6
4 Channels								
SD1234	15.0	4.0	2.7	2.1	14.1	5.9	4.5	3.7
EG1234	17.4	8.4	7.3	6.8	16.5	9.4	8.4	7.6
MR1234	18.3	8.6	7.4	6.9	17.4	9.9	8.7	7.8

7. REFERENCES

[1] J. A. Wepman, "Personal communications services technology field trials," NTIA Report 98-356, Sept. 1998.

[2] J. A. Wepman, J. R. Hoffman, L. Loew and V. S. Lawrence, "Comparison of wideband propagation in the 902-928 and 1850-1990 MHz bands in various macrocellular environments," NTIA Report 93-299, Sept. 1993.

[3] J. A. Wepman, J. R. Hoffman and L. Loew, "Impulse response measurements in the 1850-1990 MHz band in large outdoor cells," NTIA Report 94-309, June 1994.

[4] R. F. Linfield, R. W. Hubbard and L. E. Pratt, "Transmission channel characterization by impulse response measurements," OT Report 76-96, Aug. 1976.

[5] P. B. Papazian, K. Allen and M. Cotton, "A test bed for the evaluation of adaptive antennas used for mobile communications," in *Proc. IEEE Aerospace Conference*, Snowmass, CO, 1998, paper #161.

[6] J. Gibson, Ed., *The Mobile Communications Handbook*, Boca Raton, FL: CRC Press, 1996, Ch. 22.

[7] R. Steele, Ed., *Mobile Radio Communications*, New York: IEEE Press, 1995, pp. 159-163.

[8] W. C. Y. Lee, "Estimate of local average power of a mobile radio signal," *IEEE Transactions on Vehicular Technology*, VT-34, No. 1, pp. 22-27, Feb. 1985.

[9] W. Jakes, Ed., *Microwave Mobile Communications*, New York: Wiley & Sons, 1974, Ch. 5.

[10] J. Colburn, Y. Rahmat-Samii, M. Jensen and G. Pottie, "Evaluation of personal communications dual-antenna handset diversity performance," *IEEE Transactions on Vehicular Technology*, VT-47, No. 3, pp. 737-746, Aug. 1998.

[11] P. Perini and C. Holloway, "Angle and space diversity comparisons in different mobile radio environments," *IEEE Transactions on Antennas and Propagation*, AP-46, No. 6, pp. 764-775, June 1998.

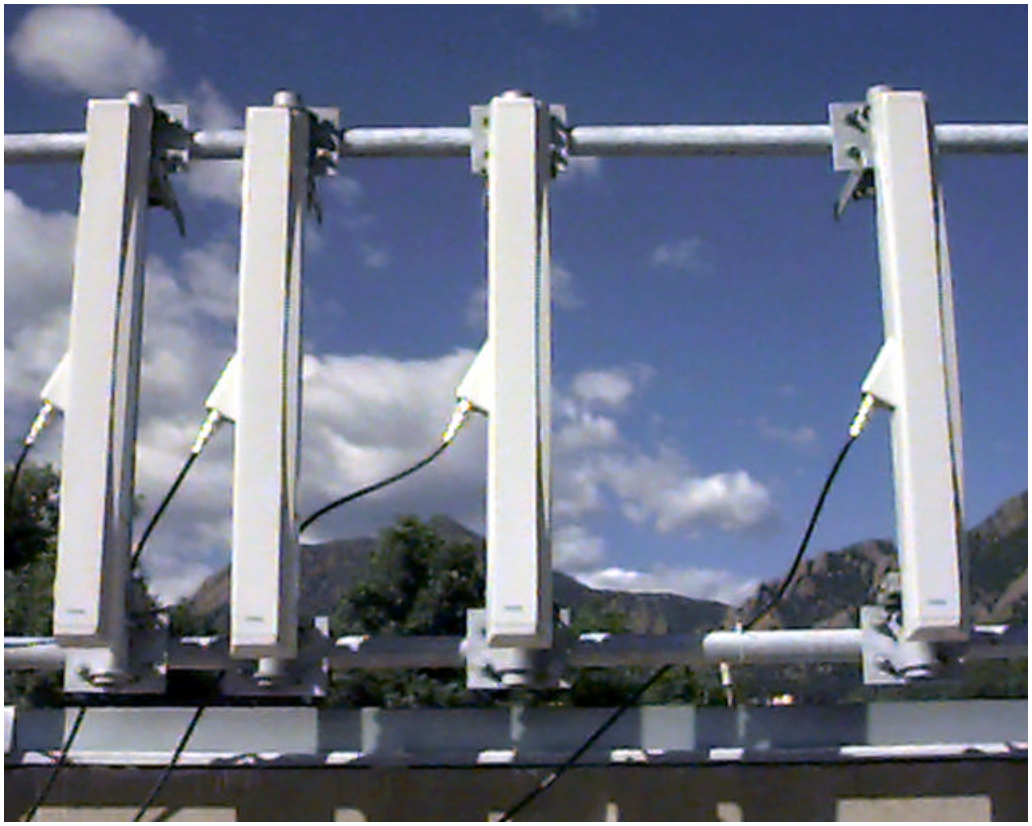

Figure 1. Four element linear antenna array spaced 2λ, 5λ, and 10λ from leftmost element.

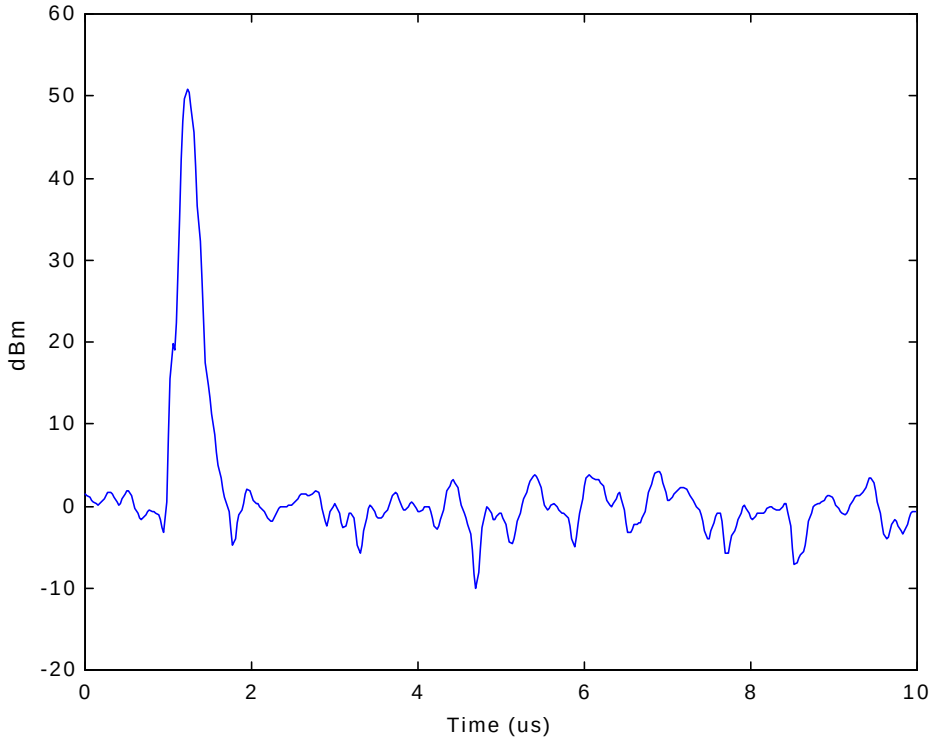

Figure 2. Sample calibration impulse.

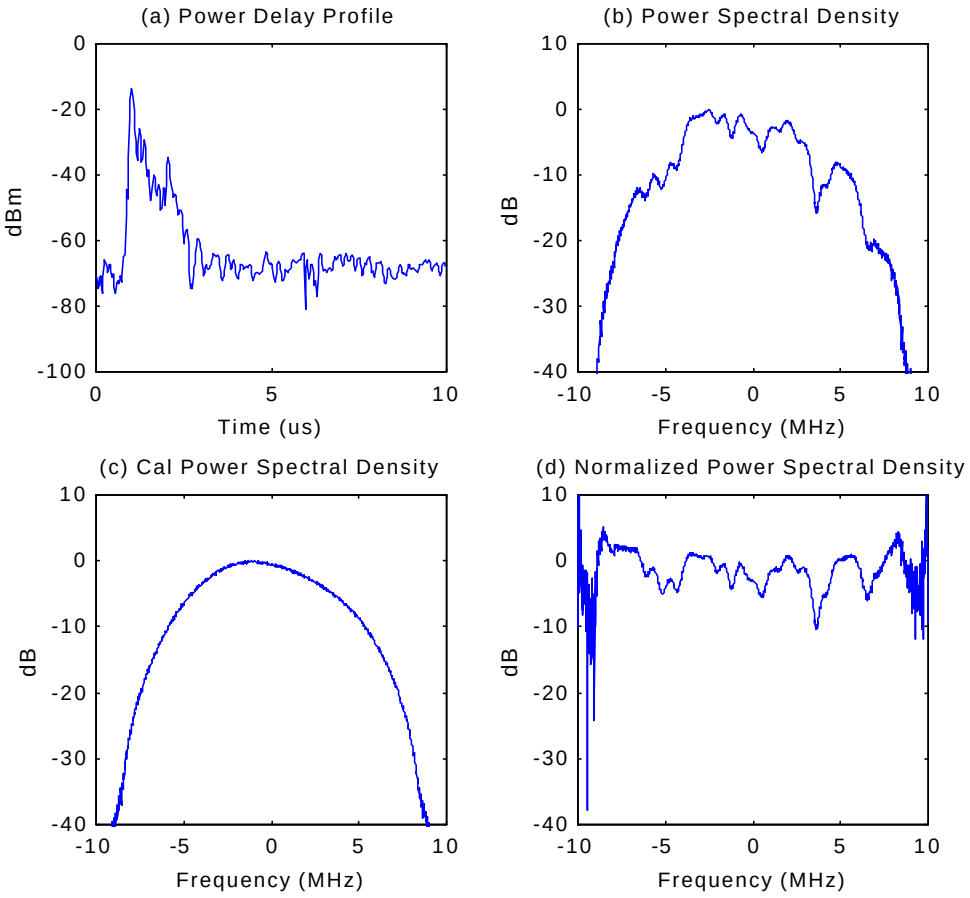

Figure 3. Example of a received impulse and the resulting normalized PSD.

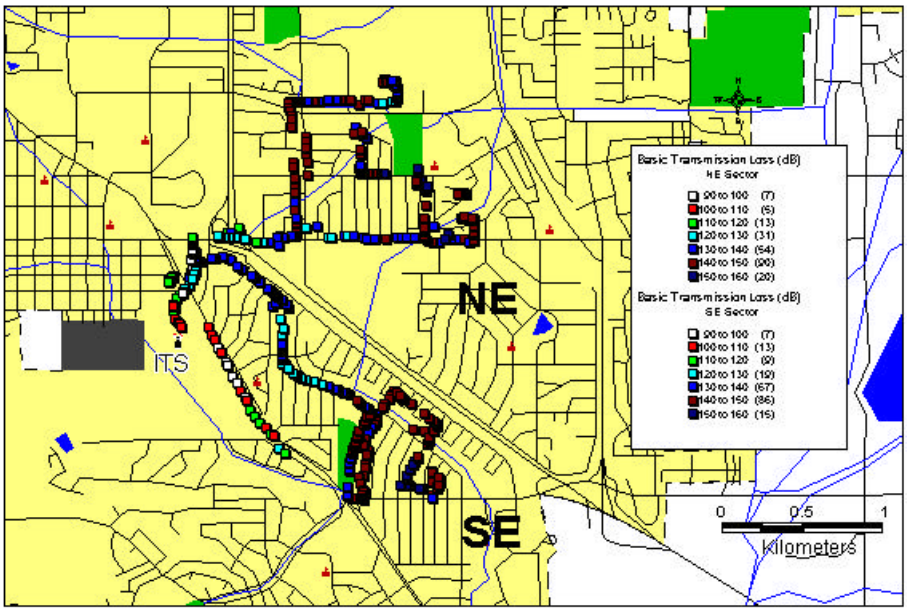

Figure 4. Drive routes and received signal strength (RSS) for NE and SE sectors of the GMM cell.

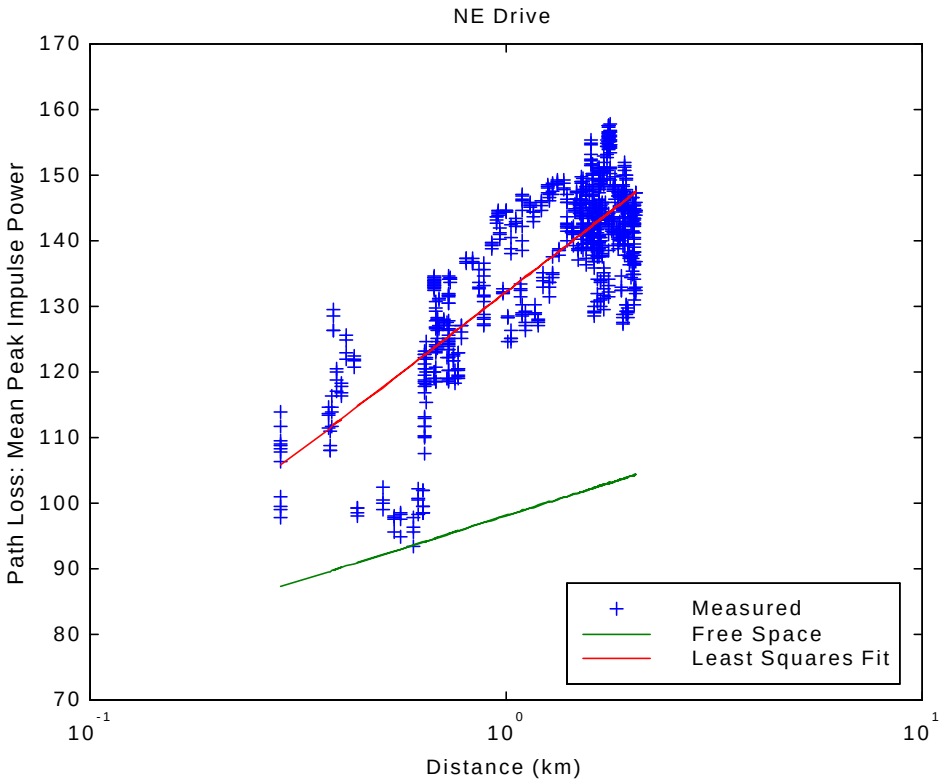

Figure 5. Path loss versus distance for the NE sector of the GMM cell. The least squares curve fit has a slope of 4.89.

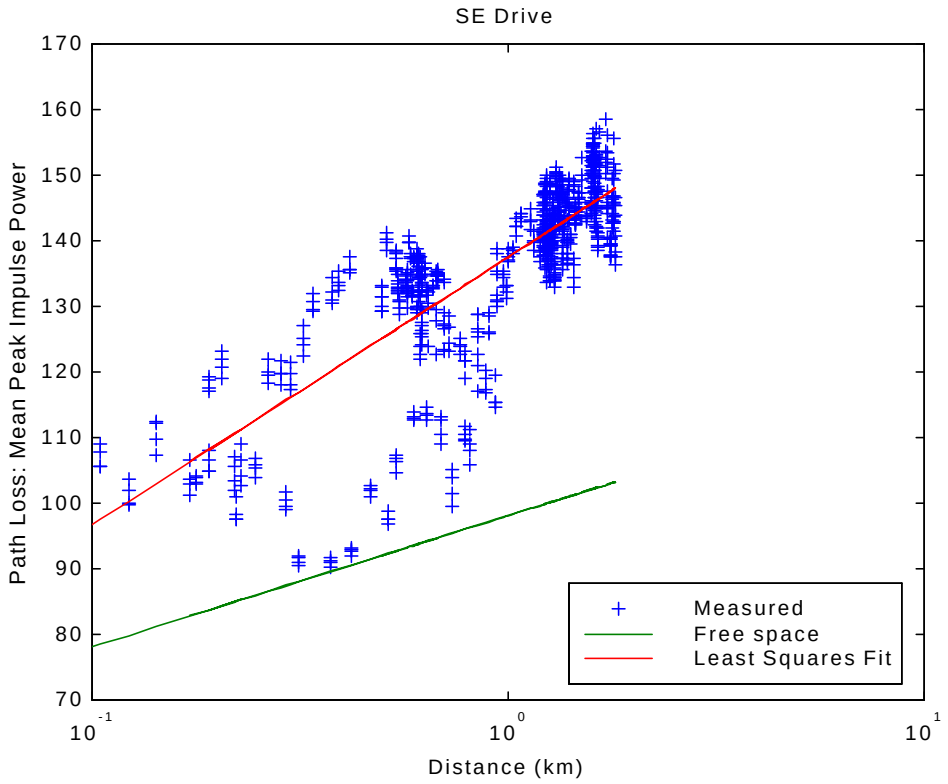

Figure 6. Path loss versus distance for the SE sector of the GMM cell. The least squares curve fit has a slope of 4.08.

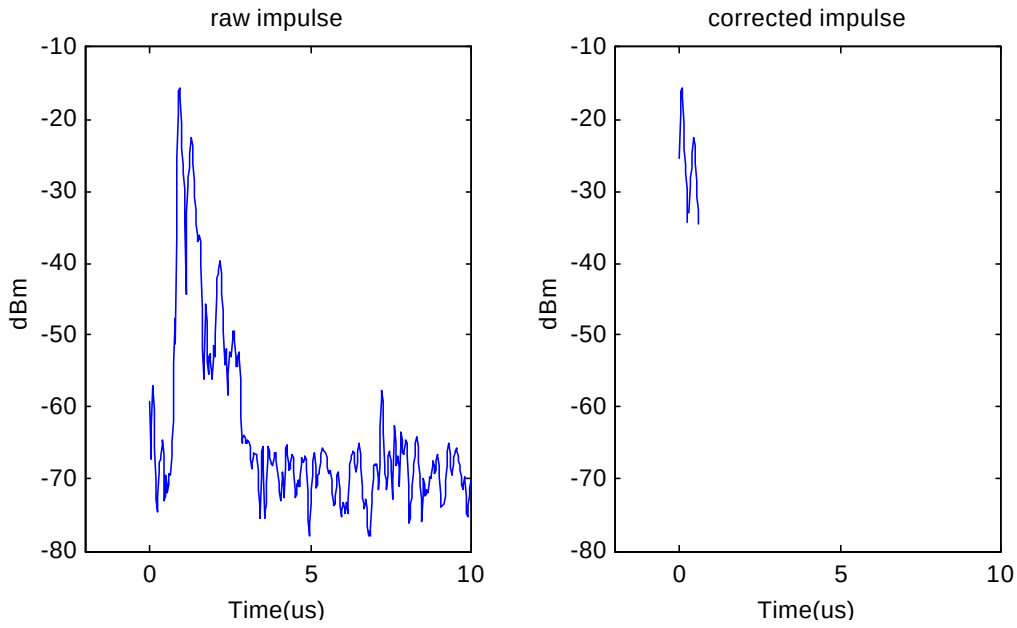

Figure 7. An example of a raw APDP and corrected APDP (NE drive, burst 1, impulse 8, channel 1). The corrected APDP consists of the signal within 20 dB of the peak signal time shifted to t = 0.

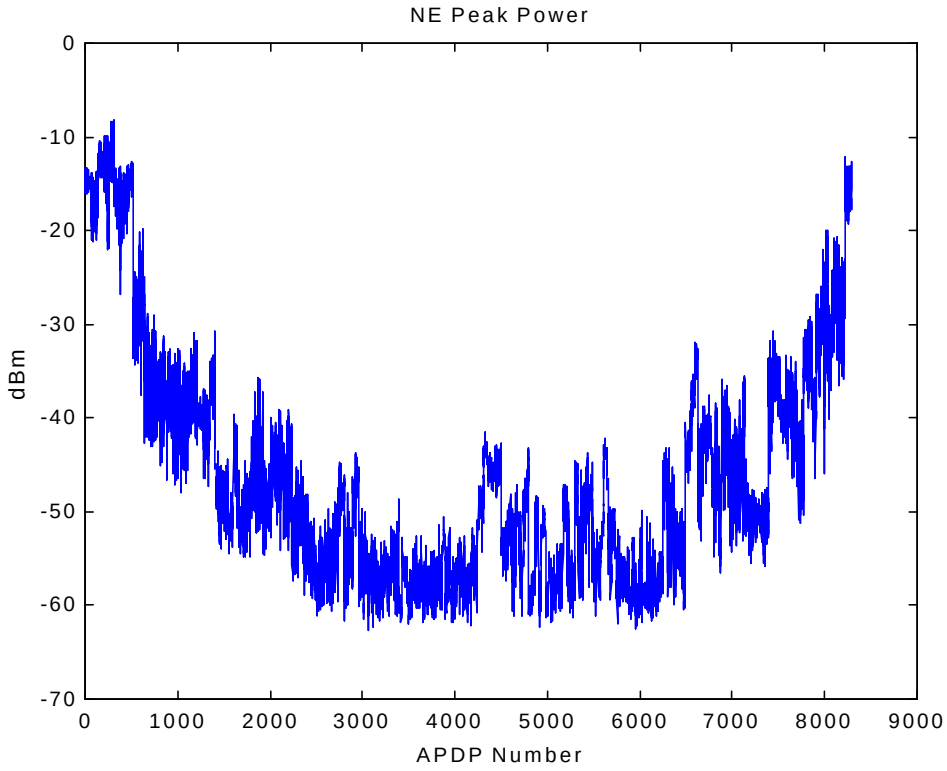

Figure 8. The peak power for the 8286 valid NE drive APDPs. The APDPs are ordered sequentially in time.

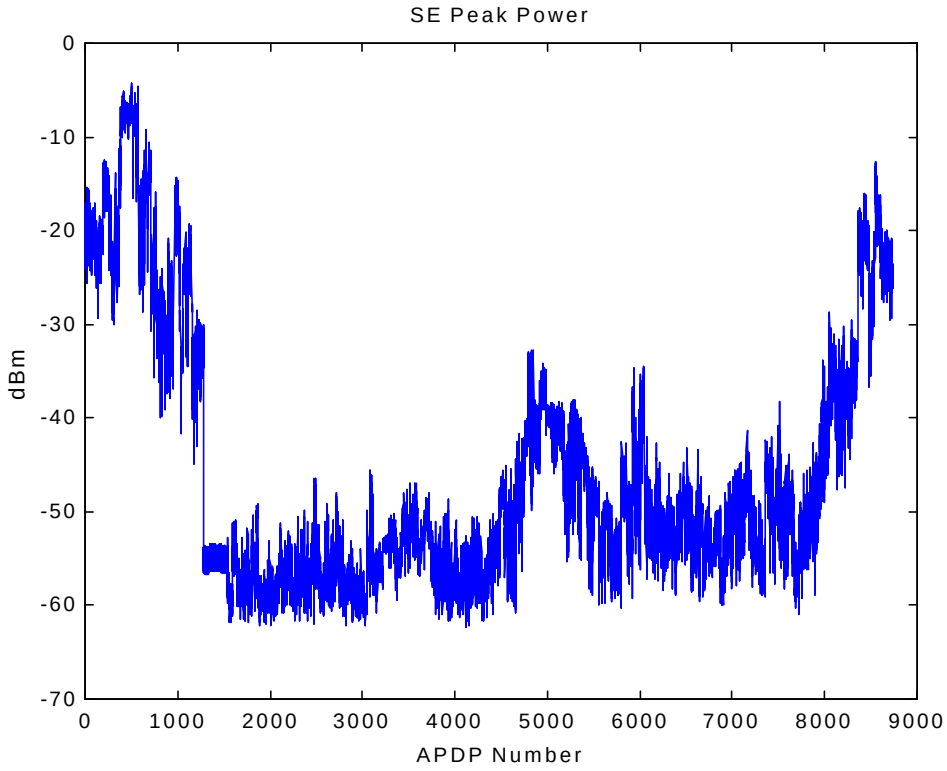

Figure 9. The peak power for the 8735 valid SE drive APDPs. The APDPs are ordered sequentially in time.

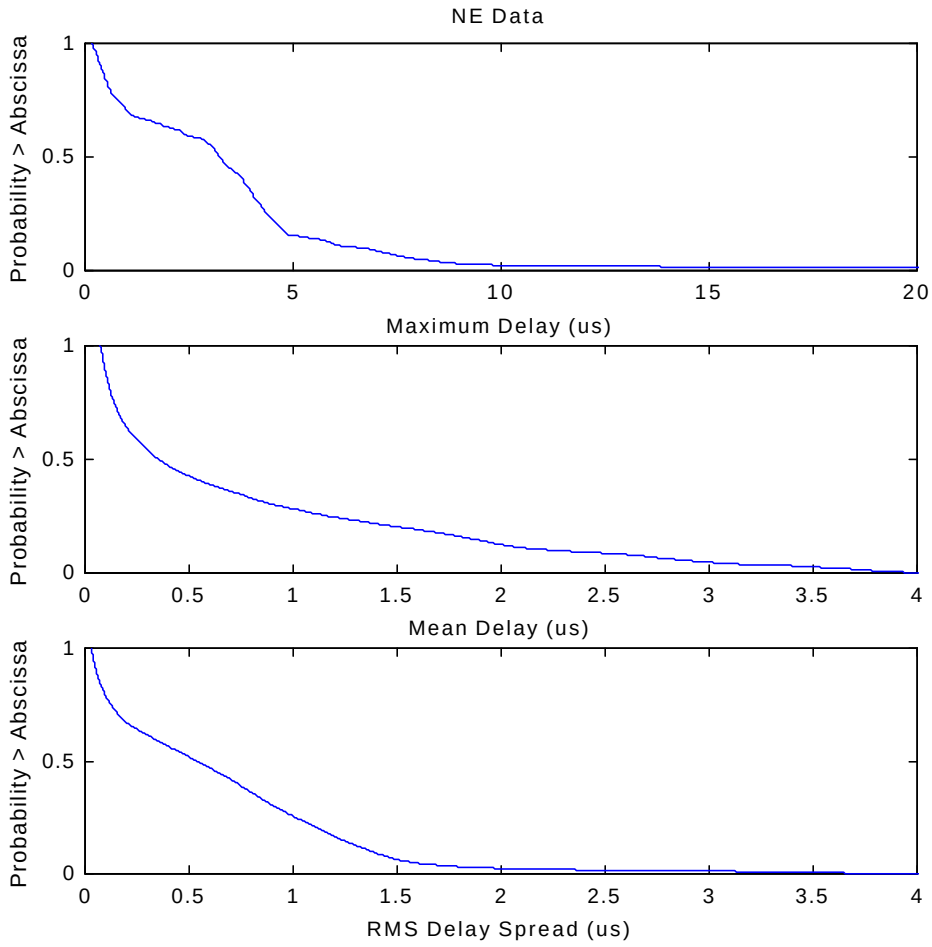

Figure 10. Delay spread statistics for the NE data set. Shown are maximum delay, mean delay, and RMS delay spread probabilities.

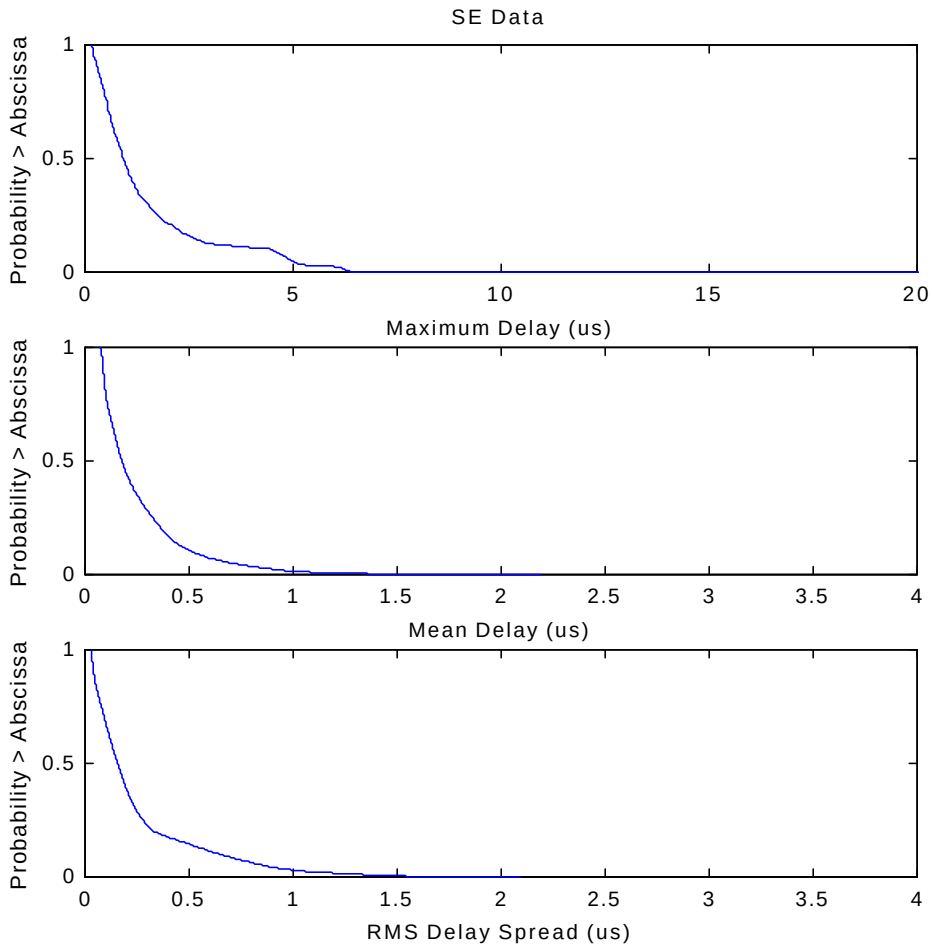

Figure 11. Delay spread statistics for the SE data set. Shown are maximum delay, mean delay, and RMS delay spread probabilities.

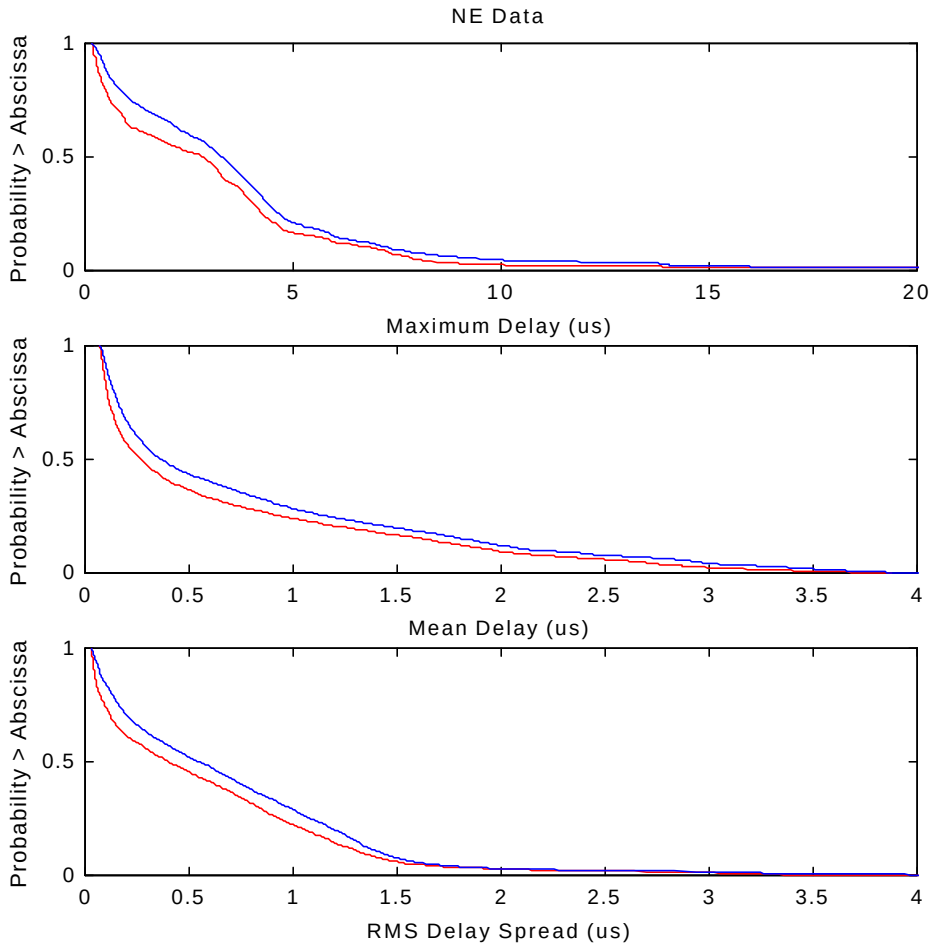

Figure 12. Diversity delay spread statistics for the NE data set. Plotted are the four channel minimum (red) and four channel mean (blue) probabilities for the maximum delay, mean delay, and RMS delay spread.

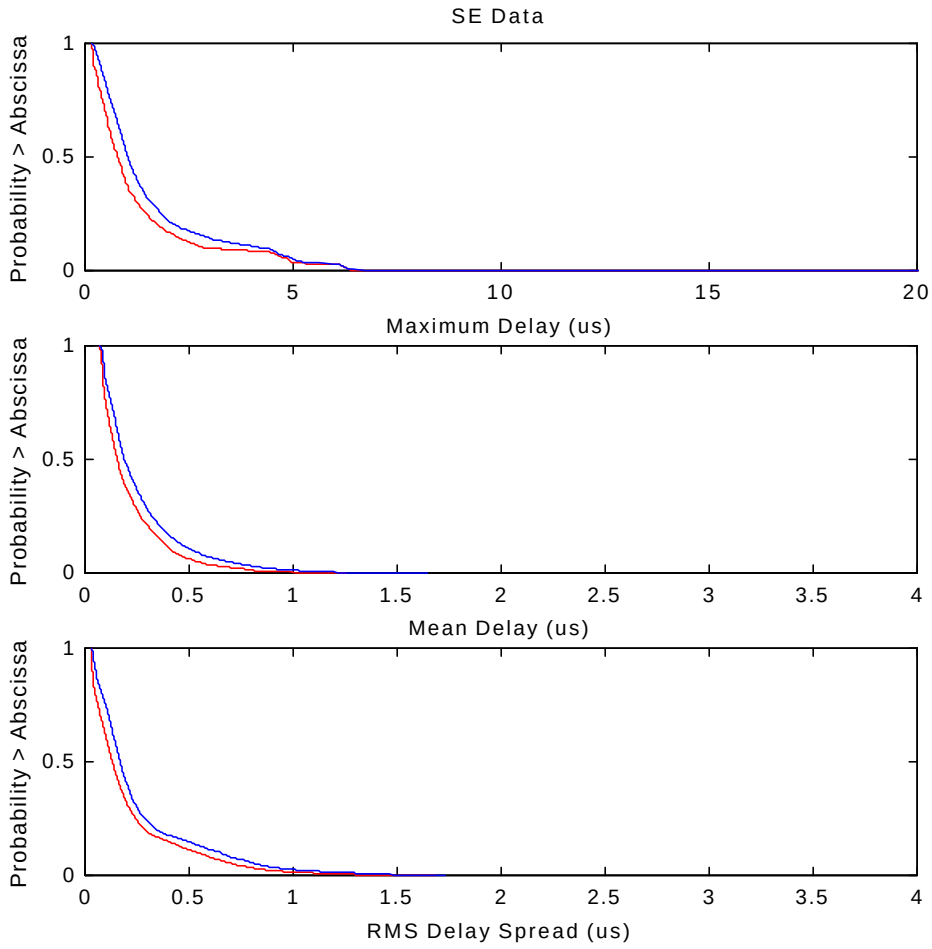

Figure 13. Diversity delay spread statistics for the SE data set. Plotted are the four channel minimum (red) and four channel mean (blue) probabilities for the maximum delay, mean delay, and RMS delay spread.

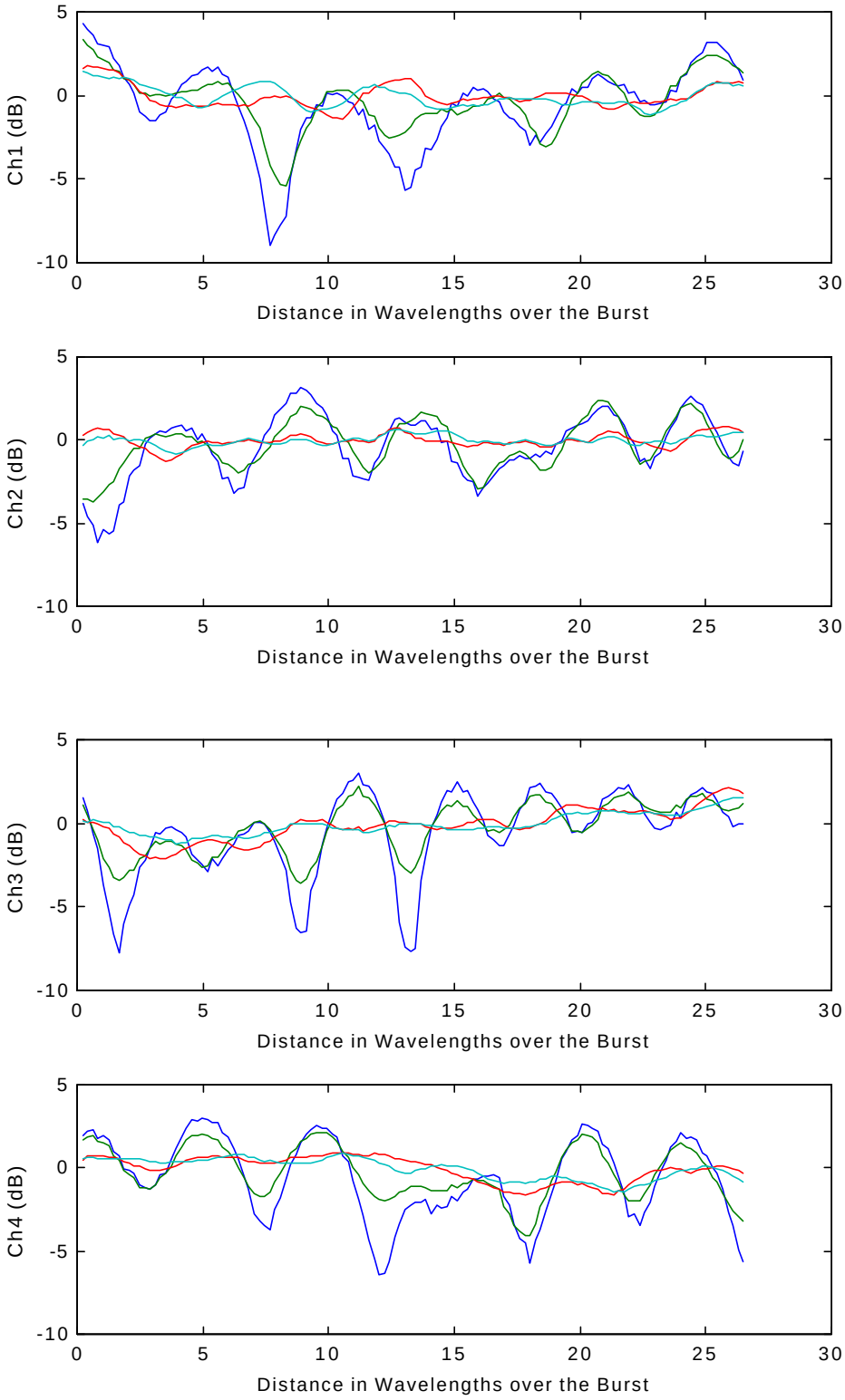

Figure 14. The normalized power spectral density for the four bandwidths (19.6 kHz-blue, 1.25 MHz-green, 5.0 MHz-red, 10 MHz-cyan) and four channels for a typical burst (NE Drive, Burst 1).

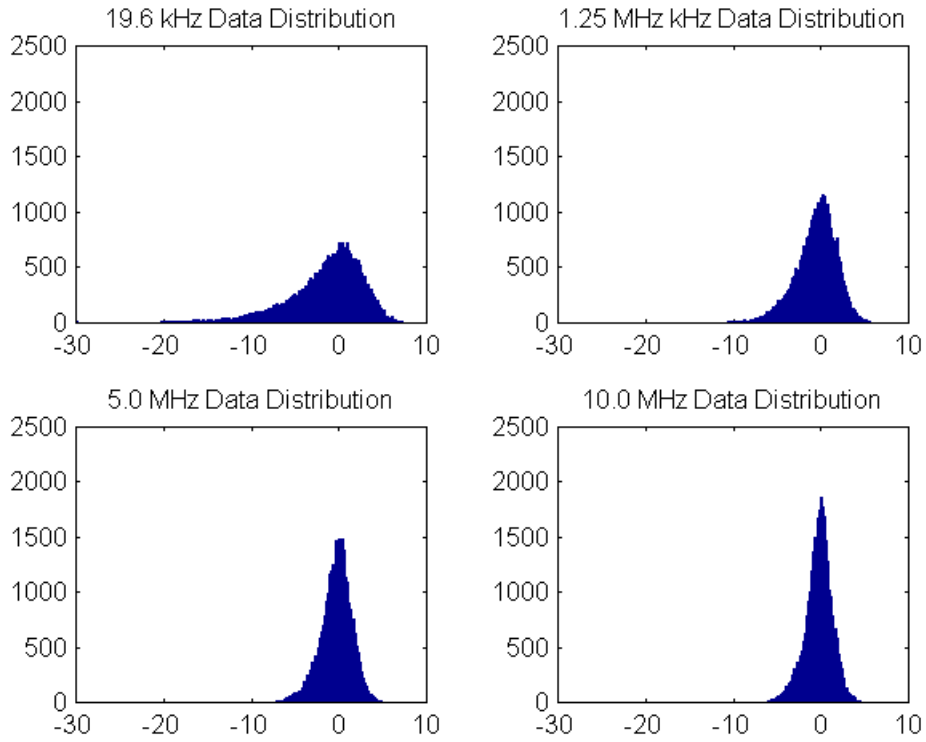

Figure 15. Distribution profiles (combined channel data) for the NE data set for the four bandwidths.

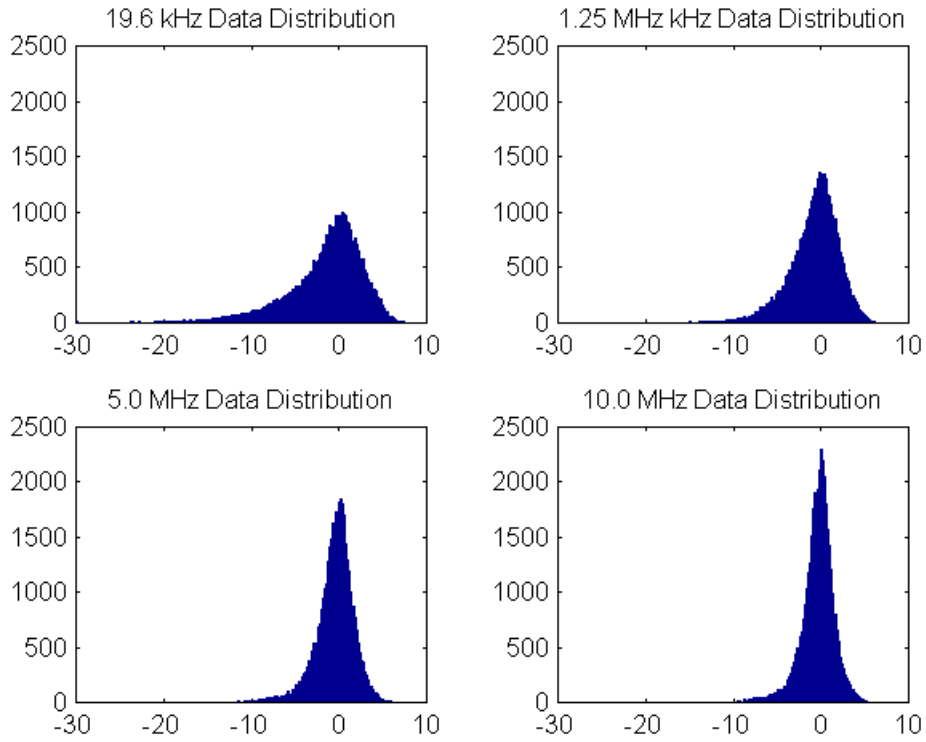

Figure 16. Distribution profiles (combined channel data) for the SE data set for the four bandwidths.

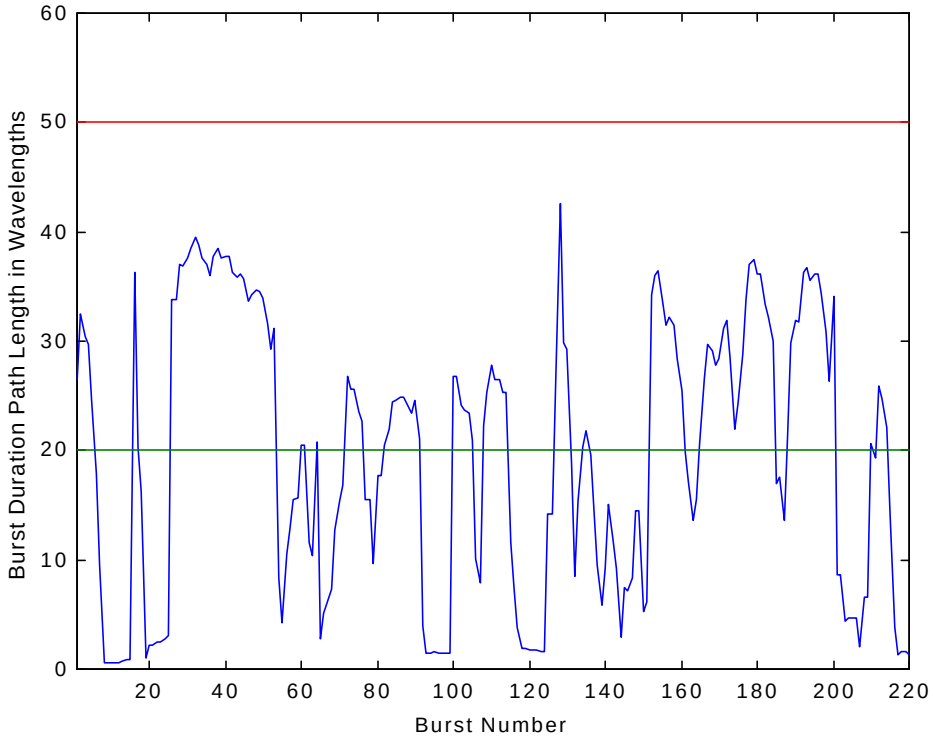

Figure 17. The path length per burst for the NE data set. 118/220 bursts are valid (in the 20-50λ range).

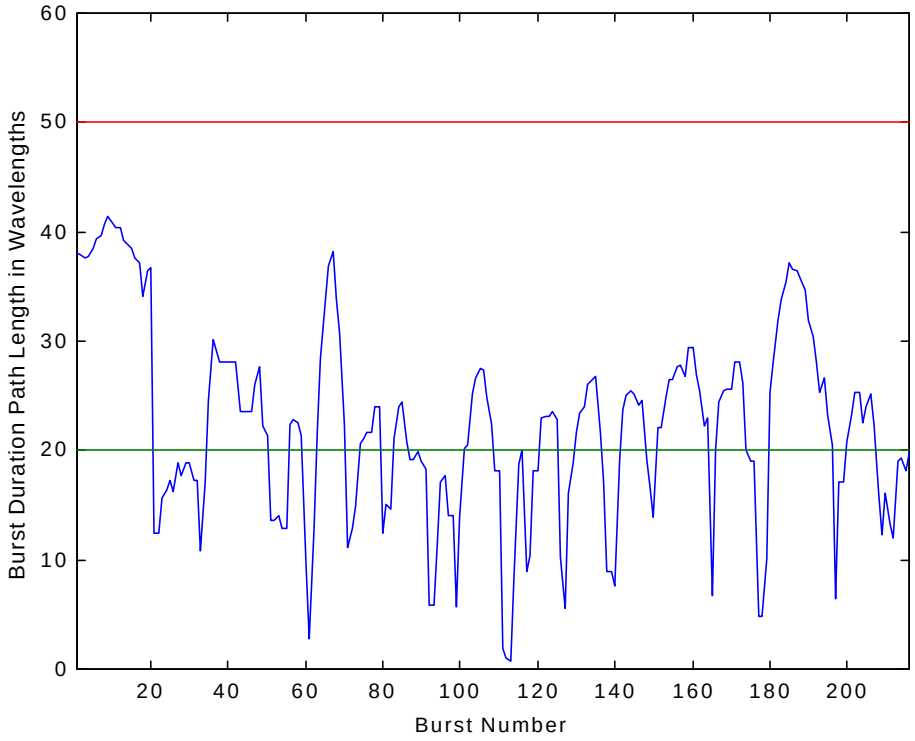

Figure 18. The path length per burst for the SE data set. 132/206 bursts are valid (in the 20-50λ range).

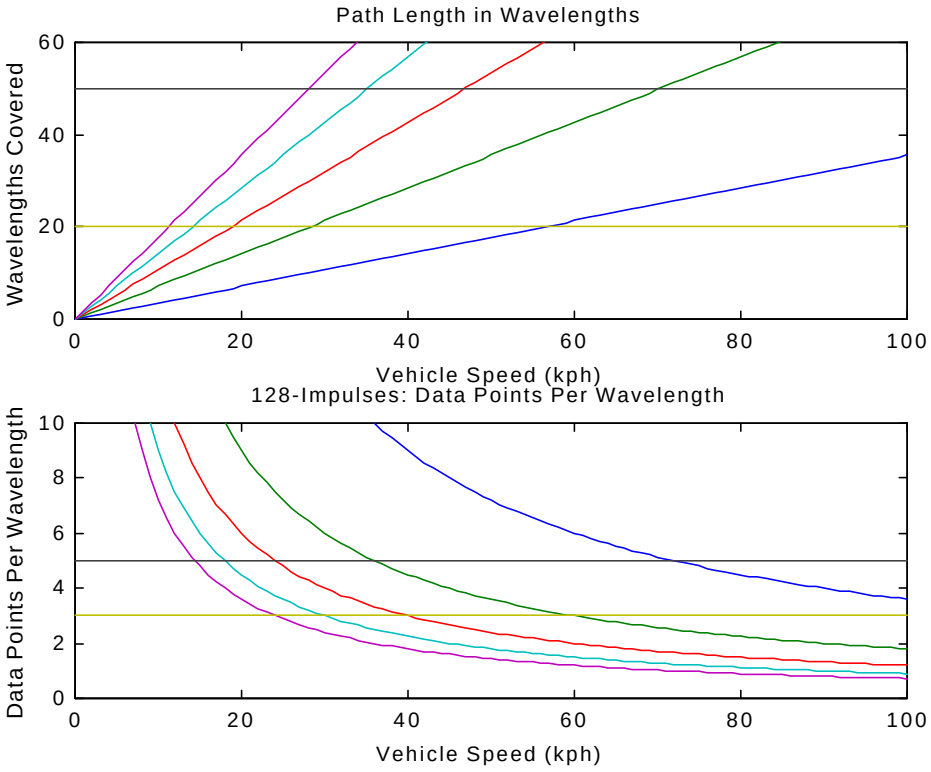

Figure 19. The straight line path length in wavelengths versus vehicle speed for burst durations of 0.2 s to 1.0 s in 0.2 s steps (upper curves) and the data points per wavelength for a 128 impulse burst for the same range of values (lower curves).

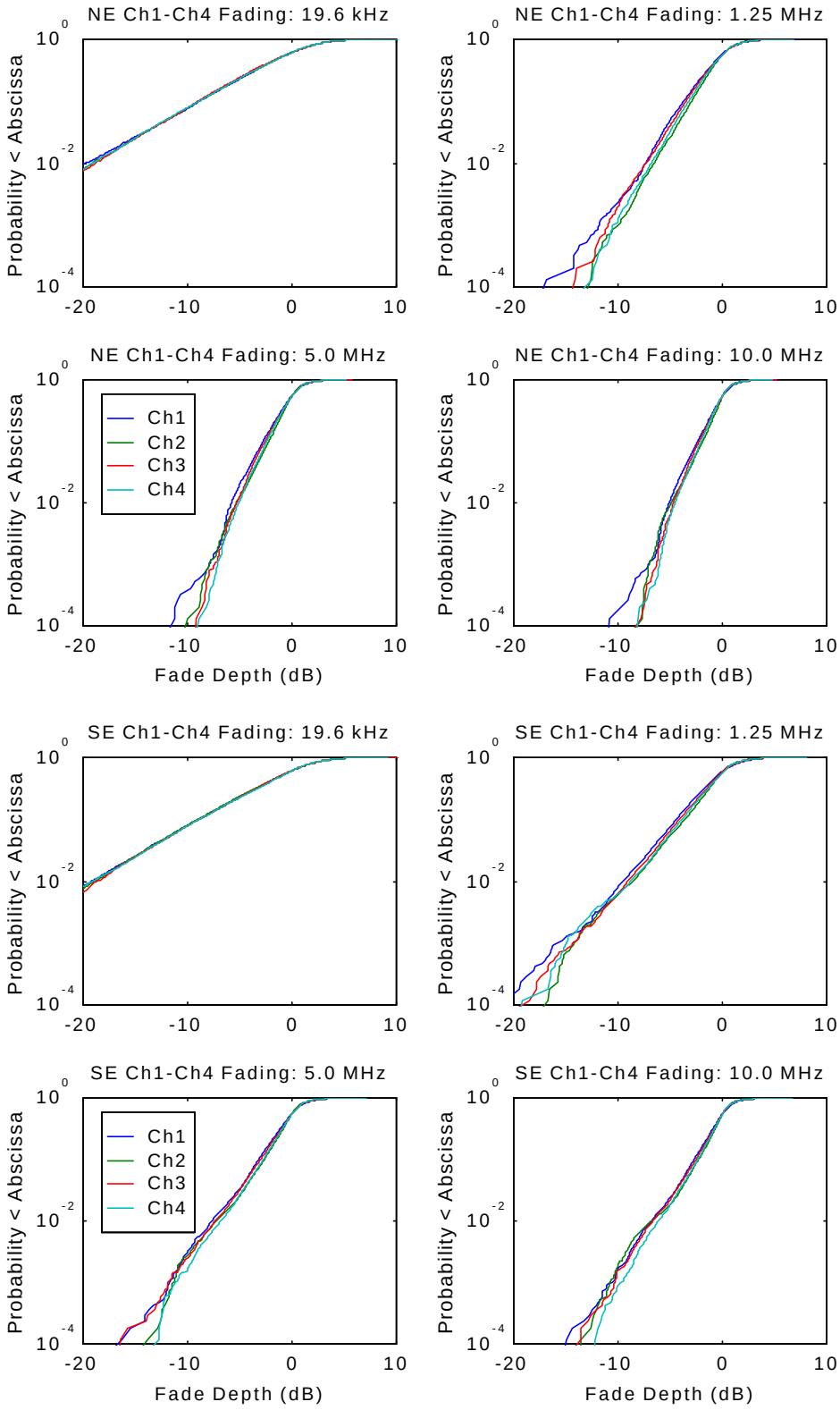

Figure 20. CDFs for channels 1-4 versus bandwidth for the NE (upper) and SE (lower) data sets.

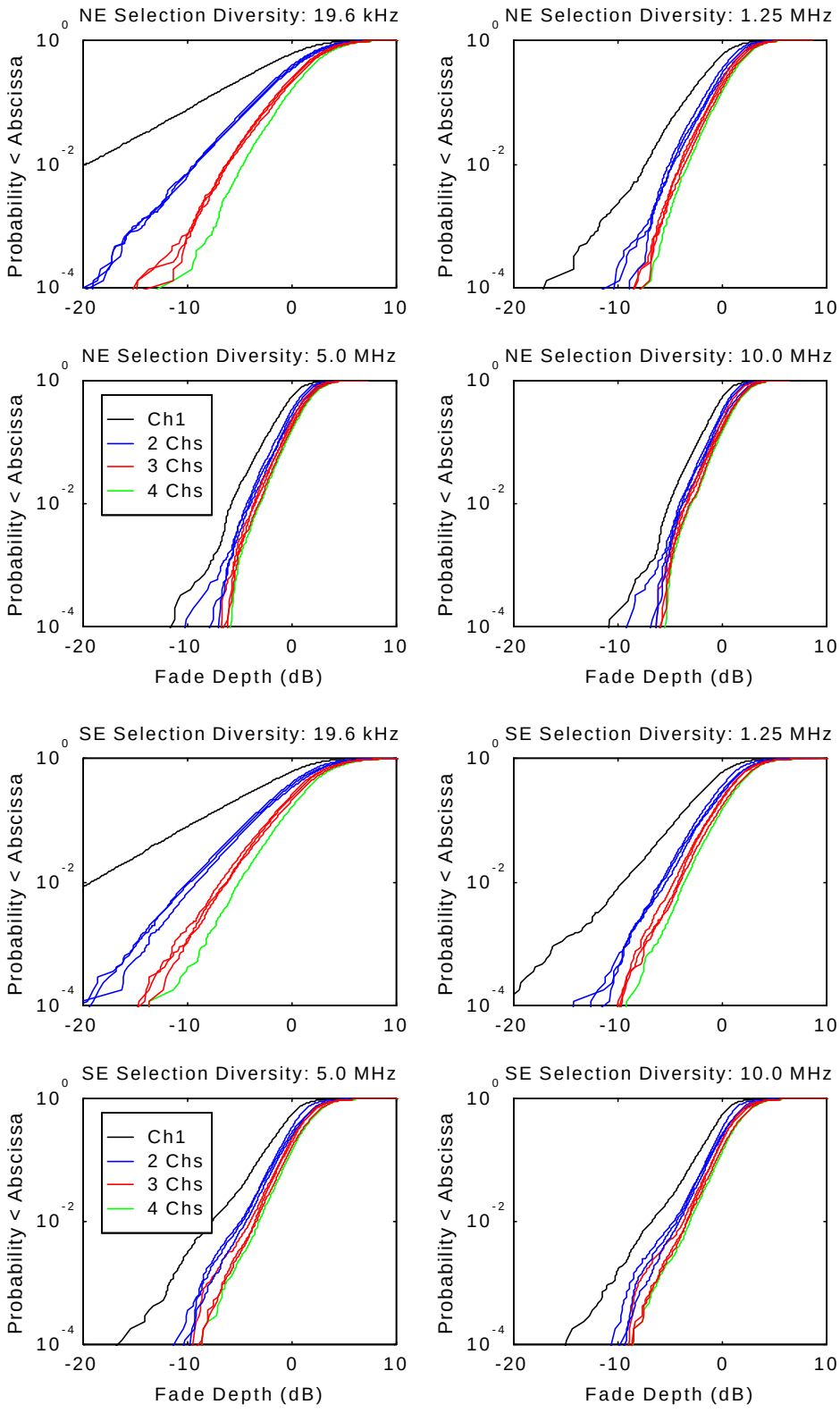

Figure 21. Selection diversity CDFs for the NE (upper) and SE (lower) data sets.

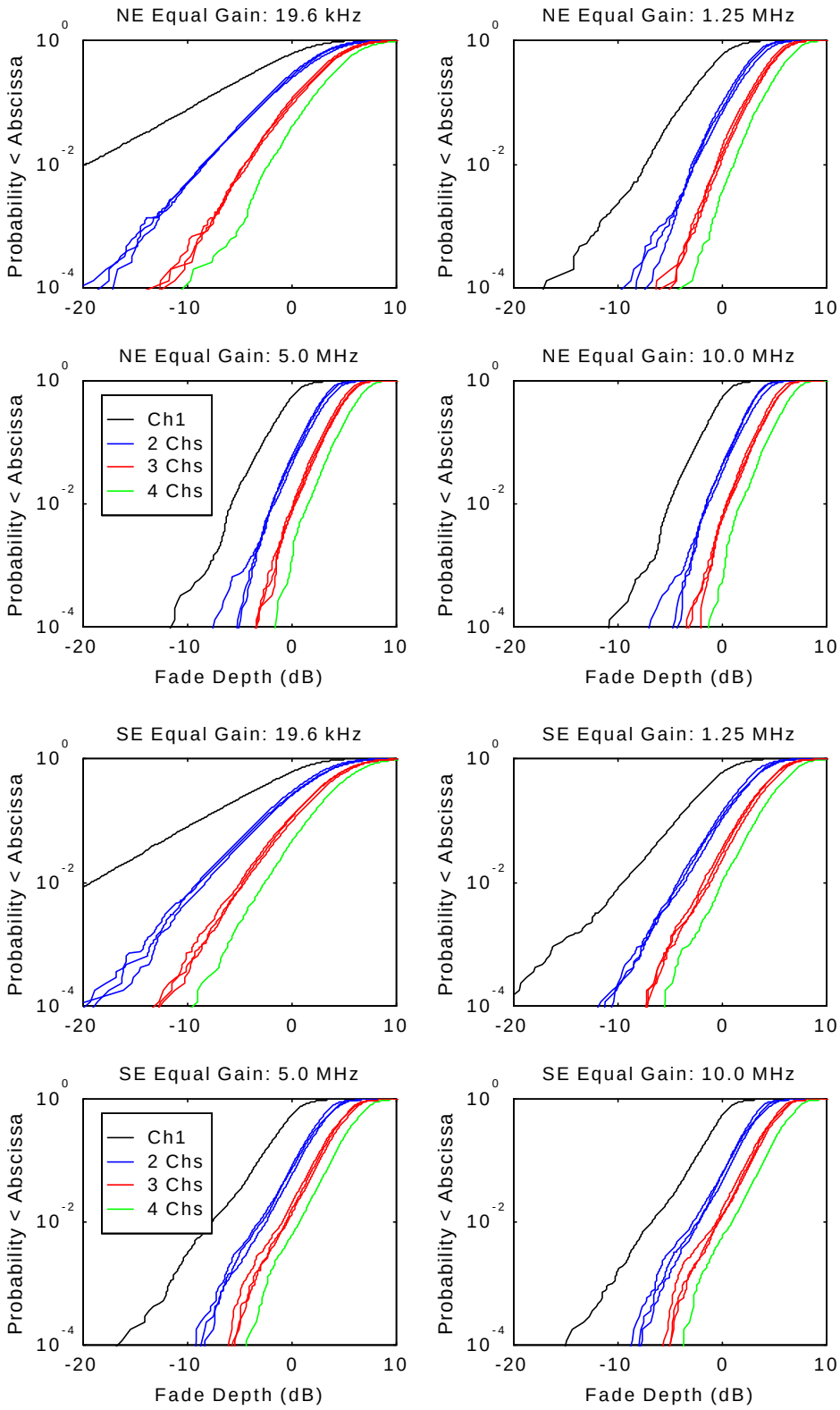

Figure 22. Equal gain diversity CDFs for the NE (upper) and SE (lower) data sets.

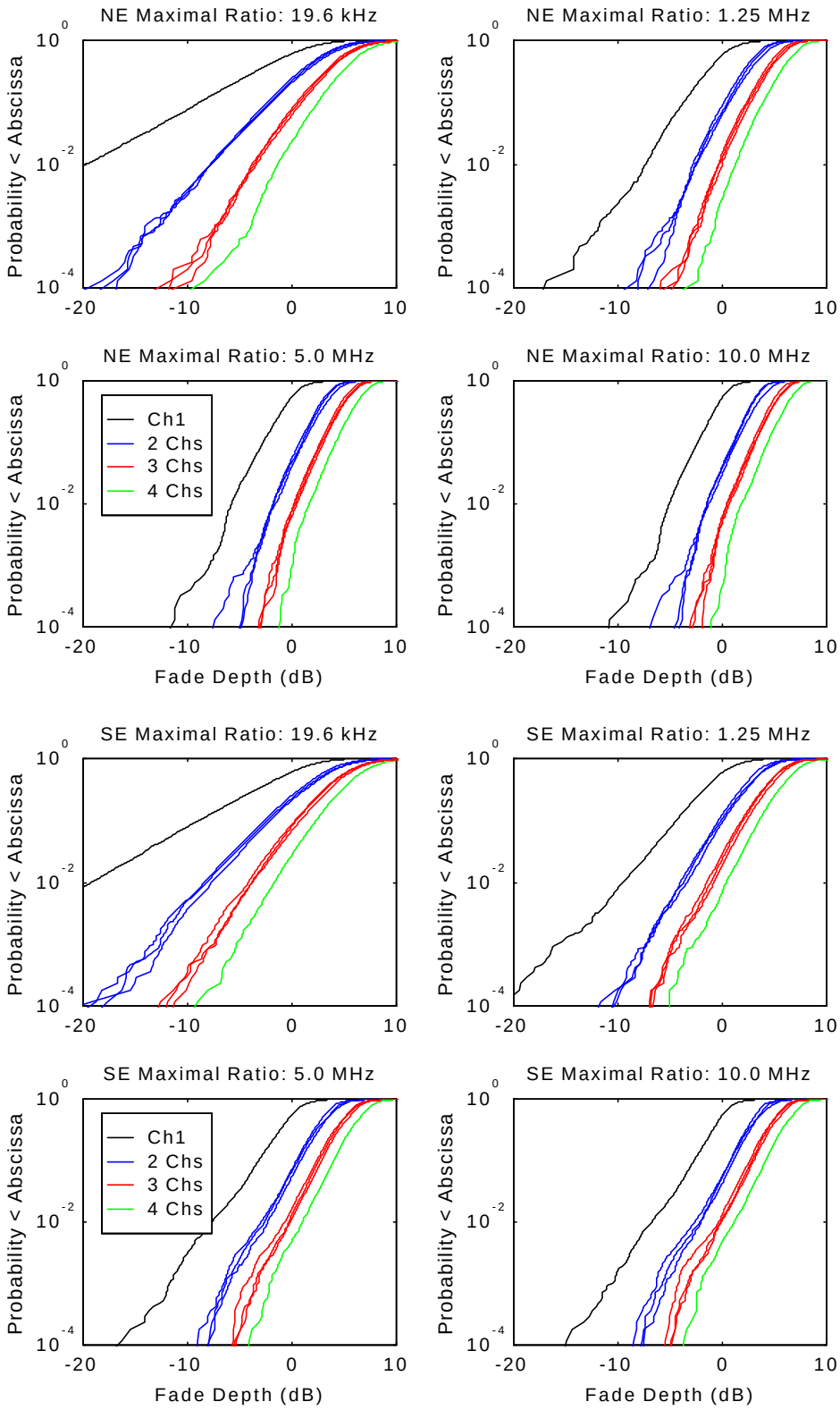

Figure 23. Maximal ratio combining diversity CDFs for the NE (upper) and SE (lower) data sets.

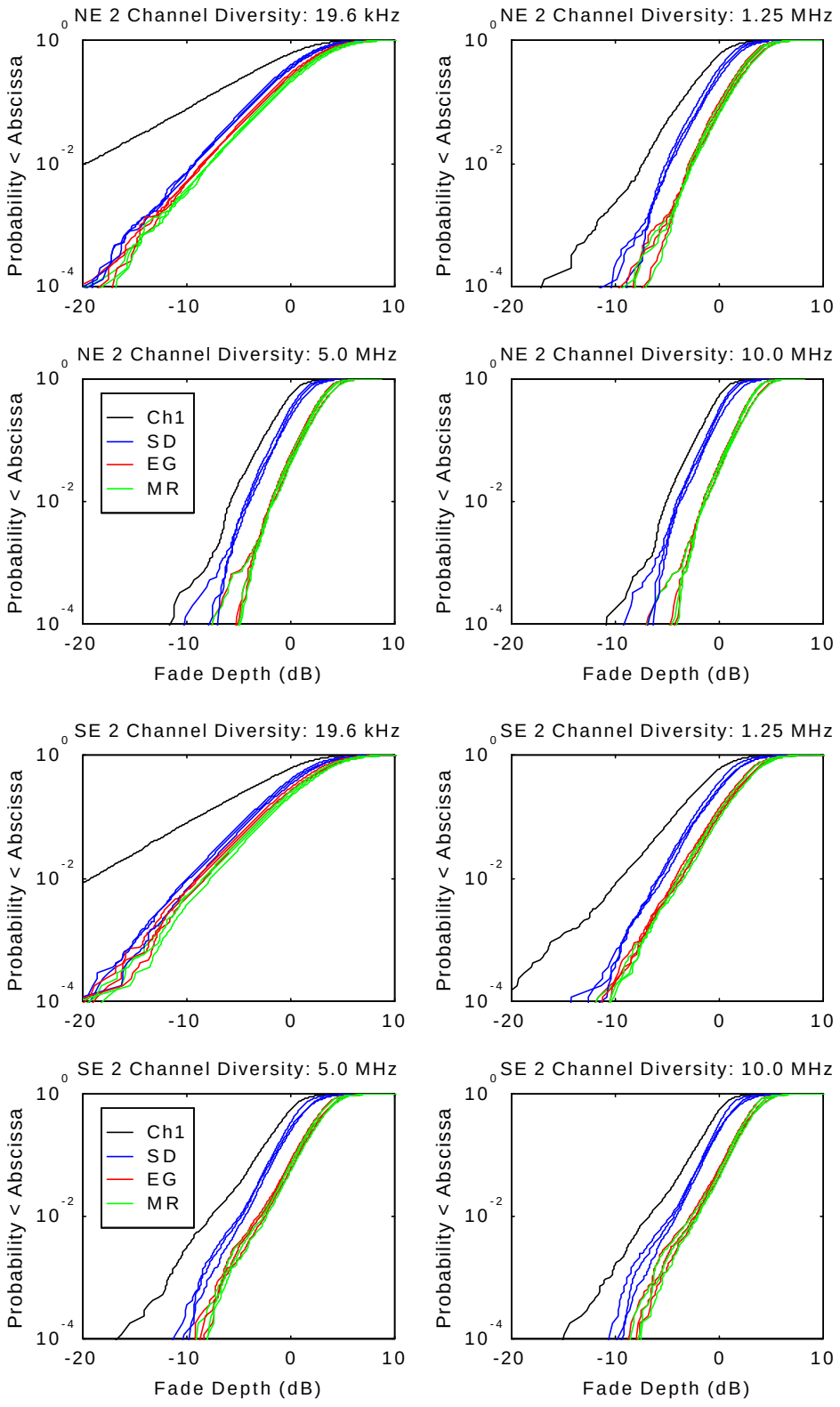

Figure 24. 2 channel diversity CDFs (ch1-blk, SD-blue, EG-r, MR-g) for the NE (upper) and SE (lower) data sets.

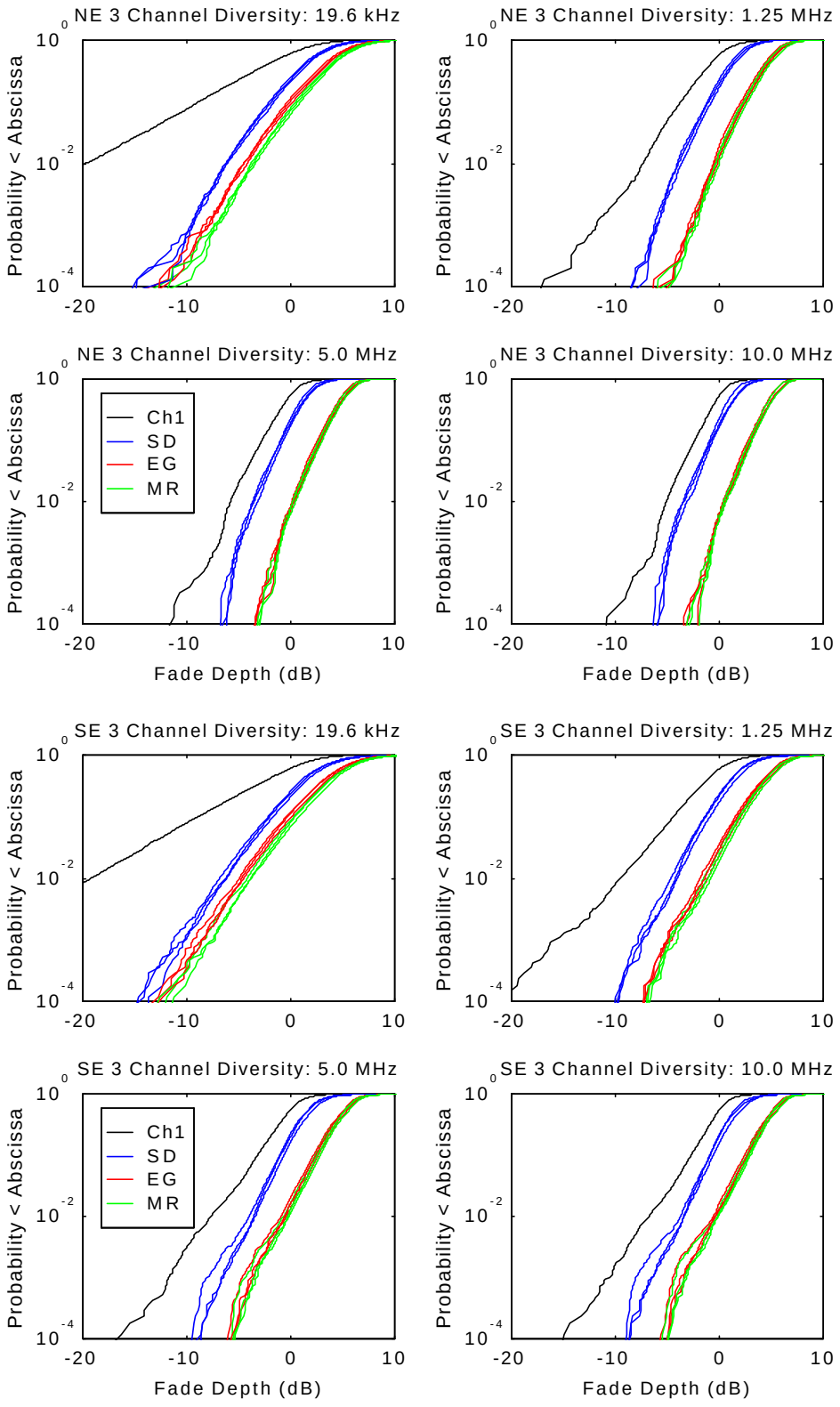

Figure 25. 3 channel diversity CDFs (ch1-blk, SD-blue, EG-r, MR-g) for the NE (upper) and SE (lower) data sets.

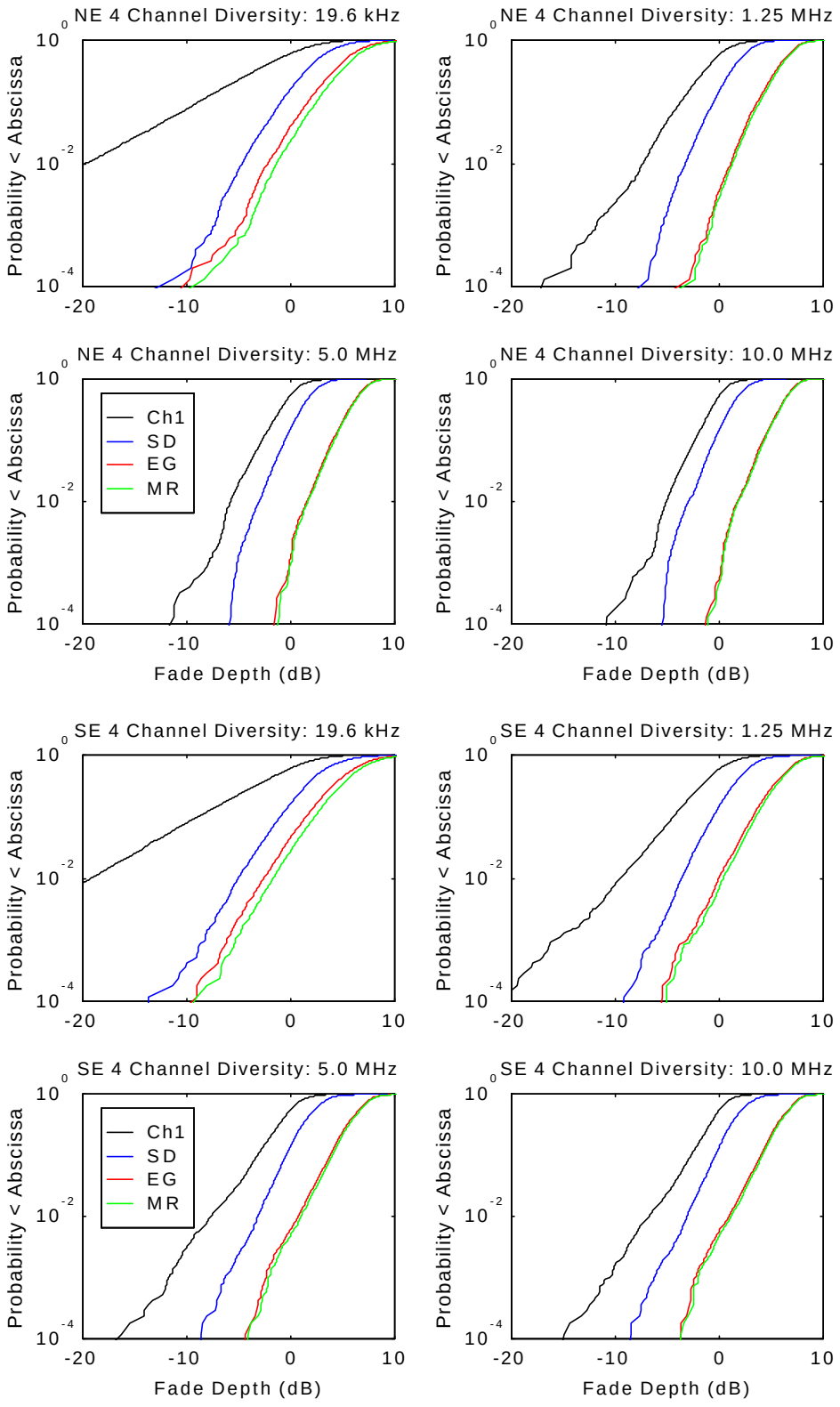

Figure 26. 4 channel diversity CDFs (ch1-blk, SD-blue, EG-r, MR-g) for the NE (upper) and SE (lower) data sets.